The Numerical Simulation of an Unbalanced Jetlet and Its Role in the Palm Sunday 1994 Tornado Outbreak in Alabama and Georgia

Michael L. Kaplan, Yuh-Lang Lin, David W. Hamilton, and Robert A. Rozumalski

Department of Marine, Earth, and Atmospheric Sciences North Carolina State University, Raleigh, North Carolina

(Manuscript received 5 November 1996, in final form 16 September 1997)

ABSTRACT

Meso-beta-scale numerical model simulations and observational data are synthesized in an effort to develop a multistage paradigm for use in forecasting tornadic convection in the southeastern United States. The case study to be utilized as an example of the multistage sequence of events is the Palm Sunday 1994 outbreak, which culminates with the development of an unbalanced mesoscale jet streak or jetlet that focuses a given region for significant values of low-level vertical wind shear, low-level confluence and vertical vorticity, mid-tropospheric cooling, and storm-relative helicity. The five-stage paradigm includes 1) the existence of a jet exit region accompanying a deep balanced thermally indirect circulation south of the outbreak and a return branch ageostrophic low-level southerly jet, both typically accompanying the subtropical jet stream and the leading edge of hot continental air; 2) the existence of a jet entrance region accompanying a deep balanced thermally direct circulation north of the outbreak and a return branch ageostrophic low-level northerly jet, both typically accompanying the polar jet stream and the leading edge of rain-cooled air; 3) the geostrophic adjustment of the wind in the southern jet to the emerging/intensifying mass field perturbation, that is, intensification of the cross-stream mesoscale pressure gradient force, caused by the juxtaposition of the rain-cooled air southeast of the polar front and hot air accompanying the continental front where evaporational cooling as well as surface heating merge resulting in unbalanced jetlet formation; 4) the low-level mass adjustment underneath the new mesoscale midtropospheric unbalanced jetlet induces a return branch low-level unbalanced jetlet as well as vertical motion patterns oriented along the stream; and 5) adiabatic cooling ahead of the unbalanced jetlet and sinking behind it accompanying the along-stream vertical circulation increases the intensity of downstream destabilization and upstream downward momentum fluxes, producing a favorable environment for severe convection.

This new synoptic/dynamical overview assigns added importance to the subtropical jet, defines the continental air front, and also defines the unbalanced jetlet for use in predicting the presevere storm environment.

1. Introduction

Jet streams have played a central role in the development of forecasting algorithms for severe weather. Among the pioneering studies of severe weather prediction were those by Fawbush et al. (1951), Browning and Donaldson (1963), Newton (1963), and House (1963). In these studies the vertical shear between a mid–upper tropospheric jet stream and a low-level jet stream were considered as key ingredients resulting in a specific region observing severe convection. The processes leading to severe convection as diagnosed from synoptic-scale datasets, including the development of low static stability and the tilting of horizontal vorticity into the vertical, were deemed to maximize within the region where the vertical wind shear was significant between the lower and middle troposphere. A plethora of forecast indices have been developed over the last 40 years wherein the vertical wind shear was included as a measure of the potential for the synoptic-scale atmosphere to support violent convection.

A more complete understanding of the dynamical relationship between the upper- and lower-level jet streams, that is, the vertical coupling of upper- and lower-tropospheric jet streams and their implication for violent convection, was derived from the synoptic/dynamical model of Uccellini and Johnson (1979, hereafter UJ79). In this model a straight jet streak, or wind maximum, within a long, typically polar, jet stream is sustained by accelerations within its entrance region due to the cross-stream pressure gradient force resulting in an isallobaric wind component. Parcels that accelerate through the core of the jet eventually turn to the right and decelerate as inertial-advective adjustments dominate within the exit region. A four-cell velocity divergence/convergence pattern develops wherein integrated velocity divergence in the left front quadrant and velocity convergence in the right front quadrant result in vertically integrated mass flux divergence/convergence tendencies and mean sea level pressure falls and rises, respectively (note Fig. 1a). Vertically varying cooling

Corresponding author address: Dr. Yuh-Lang Lin, Department of Marine, Earth, and Atmospheric Sciences, North Carolina State University, Raleigh, NC 27695-8208.
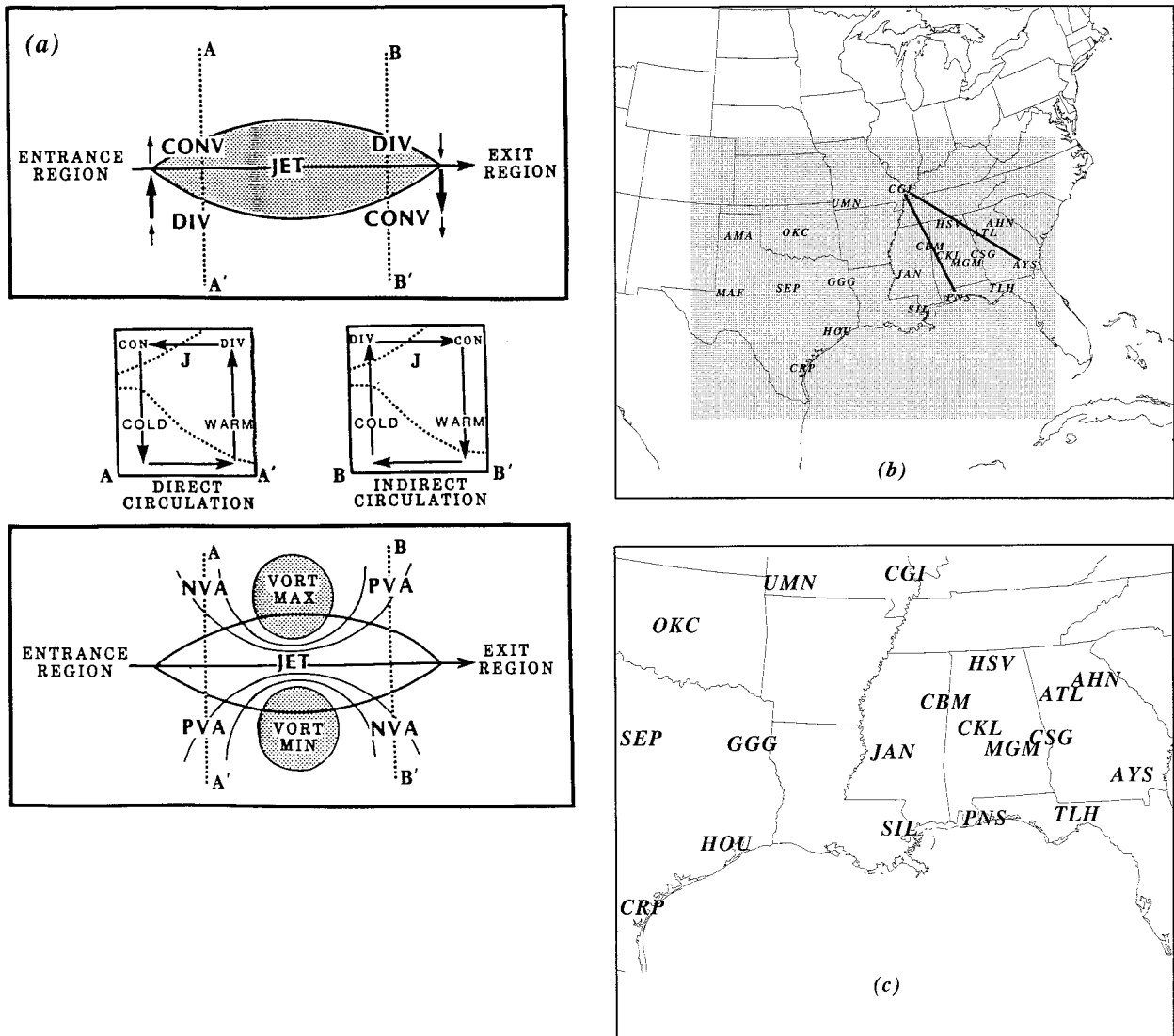E-mail: yl_lin@ncsu.edu

FIG. 1. (a) Schematic depiction of straight jet streak circulations from Uccellini and Johnson (1979). (b) Coarse-mesh (entire region) and fine-mesh (inner stippled region) matrices over which the MASS model is integrated. Thick solid lines represent the location of the Pensacola, Florida (PNS)–Cape Girardeau, Missouri (CGI), vertical cross section depicted in Figs. 4, 12, and 27 and the Waycross, Georgia (AYS)–CGI vertical cross section depicted in Fig. 10. Referenced station identifiers are also indicated. (c) Surface station identifier map focusing on the region of simulated unbalanced jetlet dynamics during the 1200–1800 UTC time period.

and warming patterns due to adiabatic expansion and compression, respectively, sustain thermal wind balance by producing cross-stream temperature gradients consistent with a thermally indirect secondary circulation within the exit region and thermally direct secondary circulation within the entrance region. Warm advection is occurring within veering vertical winds and cold advection is occurring within backing vertical winds under the exit and entrance regions, respectively. Low-level pressure rises under the right exit region and pressure falls under the left exit region induce a leftward-directed cross-stream pressure gradient force and low-level return branch circulation/ageostrophic component accom-

panying the isallobaric wind. This results in the transport of relatively warm moist air under the ascending left front quadrant and substantial destabilization.

This model is consistent with straight jet streaks or rotational wind maxima with characteristic length scales of >1000 km and periods of 24–48 h. Furthermore, the vertical motion patterns accompanying the four-cell pattern are consistent with quasigeostrophic theory where upward increasing positive vorticity advection and the Laplacian of warm advection coincide with the maximum vertical wind shear and dynamical destabilization within the left front quadrant of the jet streak. Thus, the UJ79 paradigm could be applied as a viable paradigm
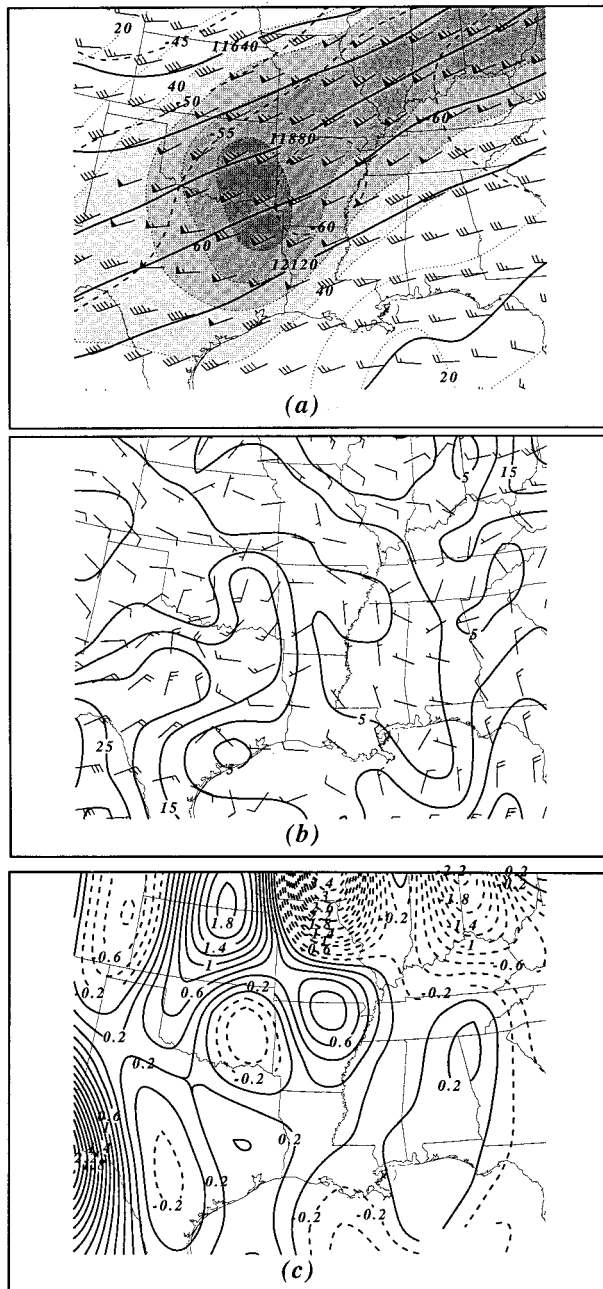
FIG. 2. (a) Rawinsonde-derived 200-mb total wind isotachs (maxima shaded in m s^{-1}) and wind barbs (m s^{-1}). Isoheights solid in meters and temperatures dashed in °C. (b) Rawinsonde-derived 200-mb ageostrophic wind isotachs (m s^{-1}) and wind barbs. (c) Rawinsonde-derived 200-mb **Q**-vector convergence (dashed) and divergence (solid) all valid at 1200 UTC 27 March 1994.

FIG. 3. (a) Rawinsonde-derived 150-mb total wind isotachs (maxima shaded in m s^{-1}) and wind barbs (m s^{-1}). (b)–(c) Similar to Fig. 2 except for 150 mb and all valid at 1200 UTC 27 March 1994.

for the forecasting of areas of severe convective potential from synoptic-scale datasets and numerical models; that is, severe weather is anticipated just under the left exit region of the jet streak where the cold and warm fronts meet accompanying a well-developed surface cyclone. Most importantly, the vertical mass structure is
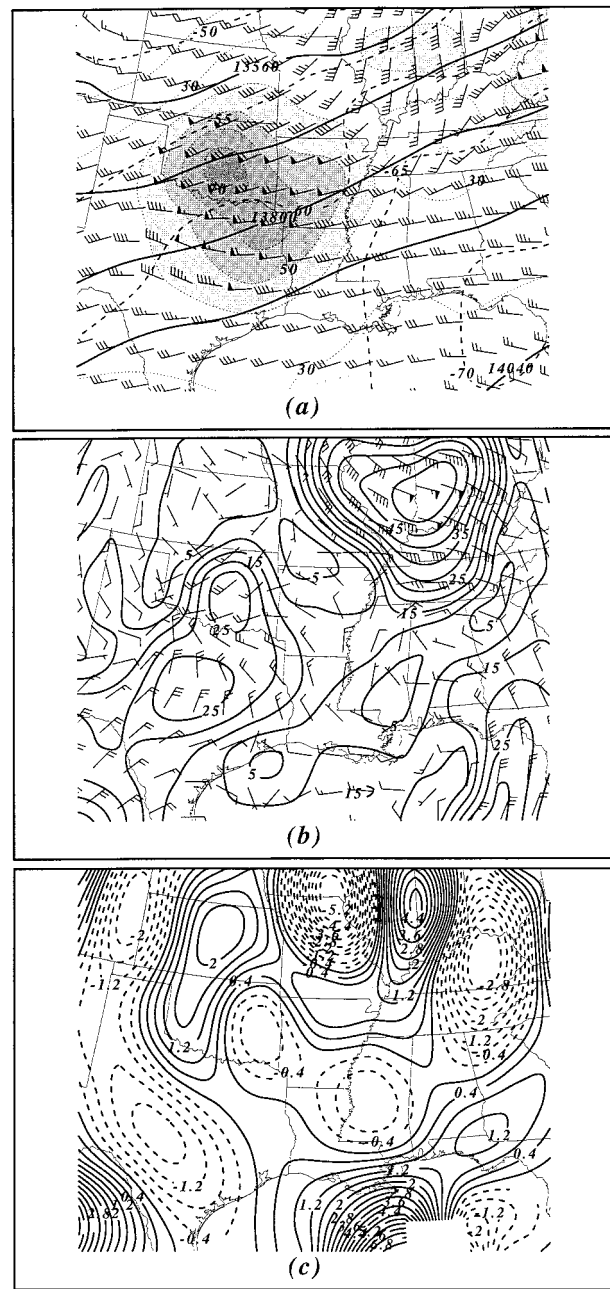
coupled to the thermal wind field through quasigeostrophic vertical motions. Therefore, the strongest vertical wind shears and destabilization occur within the decelerating mid–upper tropospheric flow since thermal wind balance is not significantly violated!

While dynamical models with refinements in the structure of jet streaks in their relationship to mid–upper tropospheric fronts and secondary circulations have

TABLE 1. Important characteristics of the MASS model version 5.8.

Numerics
- Hydrostatic primitive equation model
- 3D primitive equations for u, v, T, q, and p
- Energy absorbing upper domain sponge layer
- Coarse resolution run: 24-km grid on 170×140 grid matrix
- High-resolution run: 12-km grid on 220×170 grid matrix
- Terrain following σ–p coordinate system consisting of 34 vertical levels
- Fourth-order accurate horizontal spatial differencing
- 12-s short time step gravity wave mode (forward–backward scheme)
- 24-s long time step slow advective mode (split-explicit time marching integration employing Adams–Bashforth scheme)

Initialization scheme
- First guess provided by Global Optimum Interpolated gridded dataset
- Reanalysis using 3D OI scheme (Daley 1991)
- High-resolution average terrain using one-pass nine-point smoother
- Enhanced moisture analysis through synthetic RH retrieval scheme
- Weekly average $1° \times 1°$ lat–long SST data
- Anderson level II land use classification scheme
- Climatological subsoil moisture database
- Normalized Difference Vegetation Index (NDVI)

PBL specification
- Modified Blackadar high-resolution PBL scheme (Zang and Anthes 1982)
- Surface energy budget based upon Noilhan and Planton scheme (1989)
- Soil hydrology based upon Mahrt and Pan scheme (1984)

Moisture physics
- Grid-scale prognostic equations for cloud water and ice, rainwater, and snow
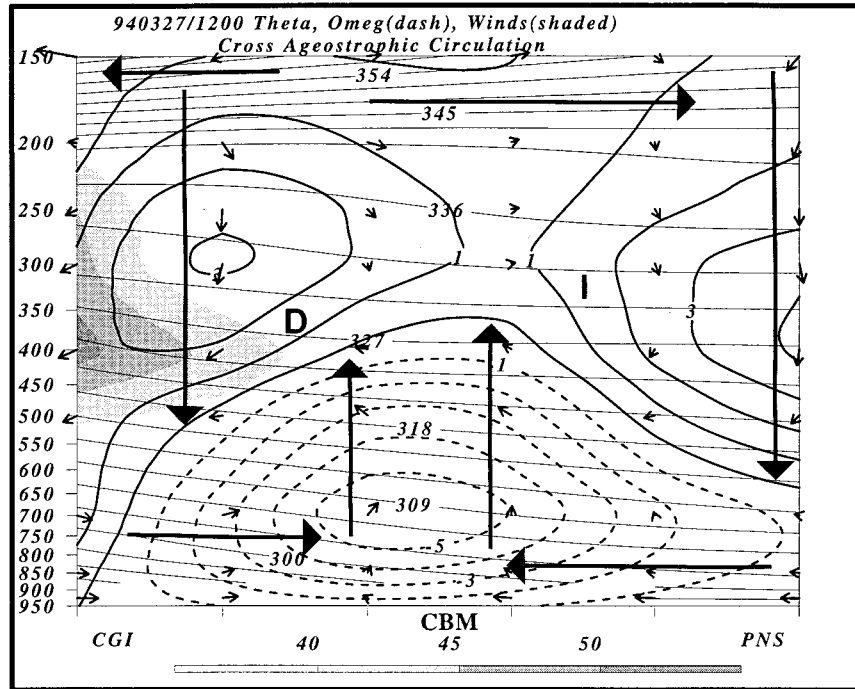- Subgrid-scale Kuo–MESO convective parameterization scheme

FIG. 4. Rawinsonde-derived vertical cross section from Cape Girardeau, Missouri (CGI), to Pensacola, Florida (PNS), of transverse ageostrophic circulation vectors, wind velocity shaded in m s^{-1}, omega (dashed upward and thick solid downward in μb s^{-1}), and θ (thin solid in K) valid at 1200 UTC 27 March 1994. See Fig. 1 for location. Thick arrows, D, and I represent structure of the ageostrophic transverse secondary circulations.

been published in recent years, for example, Shapiro (1981) and Keyser and Shapiro (1986), wherein quasigeostrophic confluence and shearing deformation accompanying flow curvature and differential thermal advection play an important role in the relationship of vertical motion patterns to the exit or entrance region of a jet streak, there has not been a widespread effort to relate these studies to violent convection nor is there any indication that the dynamics are unbalanced in any way; that is, the flow within the jet exit region is still decelerating. Additionally, the mass/momentum fields are still coupled assuming quasi- or semigeostrophic flow constraints wherein balanced, relatively low Rossby number regimes still prevail. Thus, while these dynamical changes in the relationship of jet streaks to vertical motion patterns have been observed and simulated, quasigeostrophic theory and thermal wind balance still prevail in describing the fundamental dynamics.

The complicating effects of multiple jet streaks have also been investigated. Uccellini and Kocin (1987) have related juxtaposed secondary circulations within the polar and subtropical jet streaks to the development of East Coast cyclones but have not extended their analyses to the role of these juxtaposed circulations in organizing an environment conducive to severe convection. Furthermore, Lanicci and Warner (1991a,b,c) and Whitney (1977) have related the juxtapositioning of the subtropical jet stream to the polar jet stream as a favored location for severe convection. Lanicci and Warner indicated that an elevated mixed layer (EML) accompanying "subtropical circulations" was important in organizing the severe weather environment and Whitney noted that cooling aloft accompanying the subtropical jet stream reduced the static stability of the column; however, none of these studies explained how the juxtaposed jet streak circulations and hot, dry elevated air mass from Mexico dynamically interacted to produce a favorable environment for severe convection; that is, no effort was made to diagnose the mass and momentum adjustments within the region where these jet streak and continental airmass features converged in space and time.

Two recent deadly tornadic outbreaks, both of which occurred in the southeastern United States, have raised serious questions concerning our understanding of the relationship between jet streak transverse secondary circulations and the development of severe convective storms. During the middle of the night of 28 November 1988, an F4 tornado struck Raleigh, North Carolina, as part of an outbreak of tornadoes affecting Virginia and North Carolina. This violent tornado occurred within the entrance region of a polar jet streak during late autumn and during the early morning hours thus not conforming to either the UJ79 theory or climatology. This prevented the National Weather Service from issuing any tornado watch boxes prior to the development of the tornado (Gonski et al. 1989; Kaplan et al. 1995). In a somewhat similar vein, the absence of a strong polar jet streak exit region and surface cyclone prompted the National Weather Service to deem the Palm Sunday outbreak of 27–28 March 1994 as "not a synoptically evident event." Even though the National Weather Service produced timely watch boxes over the observed severe weather outbreak region during this climatologically more favorable period, questions existed concerning the unusual synoptic location of the violent convection, again occurring closer to the polar jet streak's entrance region as opposed to the polar jet streak's exit region, thus violating the UJ79 paradigm. Given the fact that the synoptic-scale signals for these two extreme tornadic development case studies were missing or very ambiguous, it begs the question of whether we really understand the favorable hydrostatic precursor processes to violent convection in the southeastern United States or, for that matter, anywhere within the United States.

In an effort to explore this question, we will employ mesoscale numerical model simulations and observations of the Palm Sunday outbreak to formulate a new synoptic/dynamical overview for the large-scale circulation and forcing that results in an environment favorable for severe convection. The new paradigm synthesizes three primary concepts into a new vision of the hydrostatic processes resulting in severe weather, thus producing a sequence of quasigeostrophic and ageostrophic processes that differ from the previously described theories. The three concepts that form the centerpiece of this new paradigm include 1) the role of nearby transverse secondary circulations and their deep quasigeostrophic vertical motions accompanying both the polar jet streak entrance region and subtropical jet streak exit region, 2) geostrophic adjustment of the mass to the wind field in proximity to the continental air accompanying the return branch of the subtropical jet streak resulting in an unbalanced midtropospheric mesoscale jet streak or jetlet, and 3) the vertical advection of continental air accompanying the geostrophic adjustment process that produces the jetlet in 2), resulting in unbalanced along-stream circulations conducive to thermal and wind shear patterns that violate thermal wind balance thus enhancing storm-relative helicity. It should be noted that an unbalanced jetlet represents a mesoscale jet streak sustained by exit region accelerations accompanying leftward-directed cross-stream ageostrophic flow in contradistinction to the balanced flow within a jet streak exit region accompanying the UJ79 paradigm. This unbalanced flow has been described in Kaplan and Paine (1977), Uccellini et al. (1987), Uccellini and Koch (1987), Zack and Kaplan (1987), Koch and Dorian (1988), and Kaplan et al. (1997).

In the next section of the paper we will describe the numerical simulation experiment employed to better understand the sequence of processes responsible for generating the mesoscale jetlet and along-stream circulation
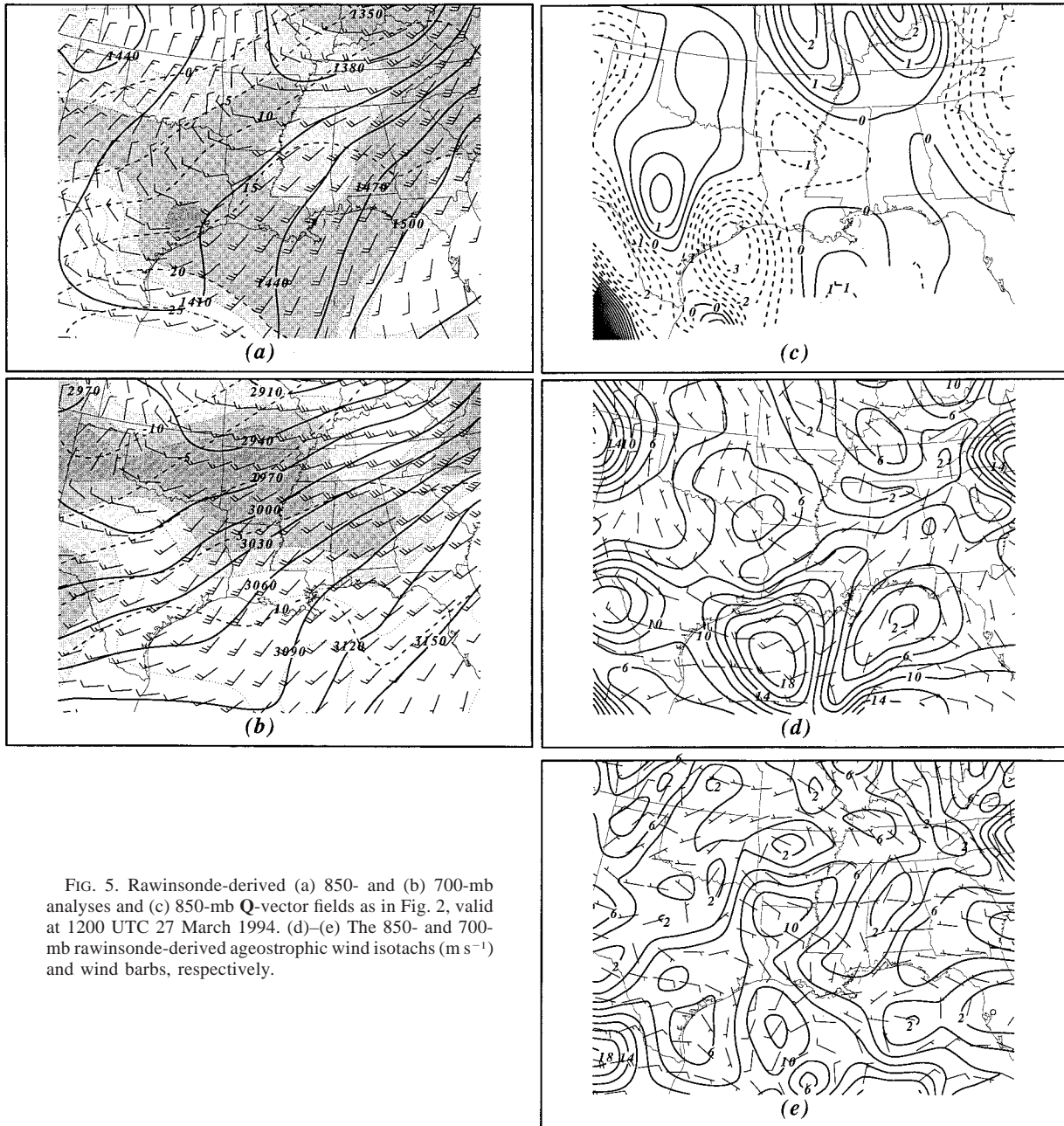
FIG. 5. Rawinsonde-derived (a) 850- and (b) 700-mb analyses and (c) 850-mb **Q**-vector fields as in Fig. 2, valid at 1200 UTC 27 March 1994. (d)–(e) The 850- and 700-mb rawinsonde-derived ageostrophic wind isotachs (m s^{-1}) and wind barbs, respectively.

that produced a favorable hydrostatic environment for severe weather over Alabama and Georgia on 27 March 1994. Section 3 will be the first of several sections that describes, employing both numerical simulations and observations, the multistage paradigm resulting in the development of a favorable severe weather environment. In this section we will diagnose the juxtaposed jet streak secondary circulations as well as an analysis of the dissimilar low-level air masses resulting in boundary layer frontogenesis. The effect of the low-level return branch circulations accompanying very different air masses and total frontogenesis forced by ageostroph-

ic confluence and differential diabatic heating is examined. Section 4 follows by diagnosing from model output the effect of said processes on the development of a midtropospheric subgeostrophic region accompanying the intensifying boundary between the low-level cool and hot air masses. The implications of this subgeostrophy for unbalanced jetlet development accompanying leftward-directed cross-stream ageostrophic flow are examined. Section 5 will focus on the circulation accompanying the jetlet and the implications for the development of storm-relative helicity and vertical vorticity. In section 6 we will summarize our results
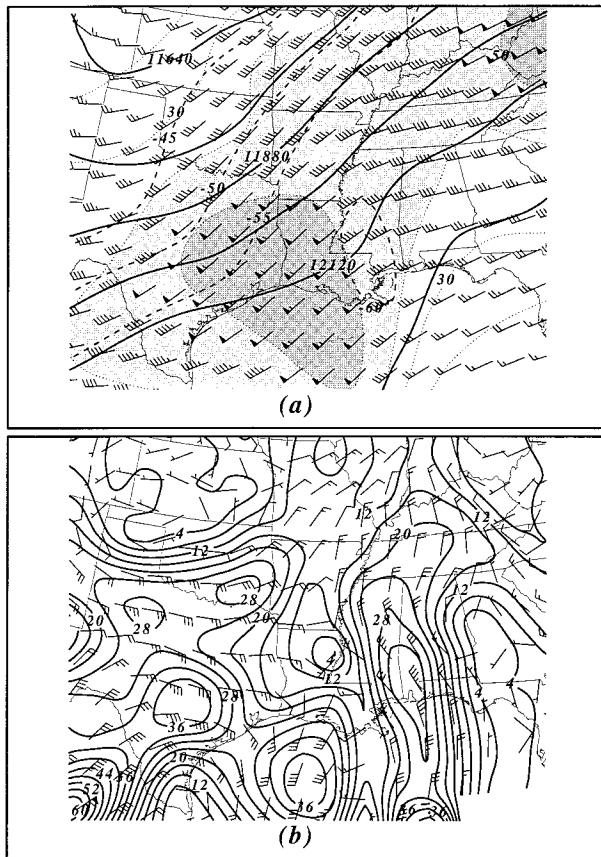
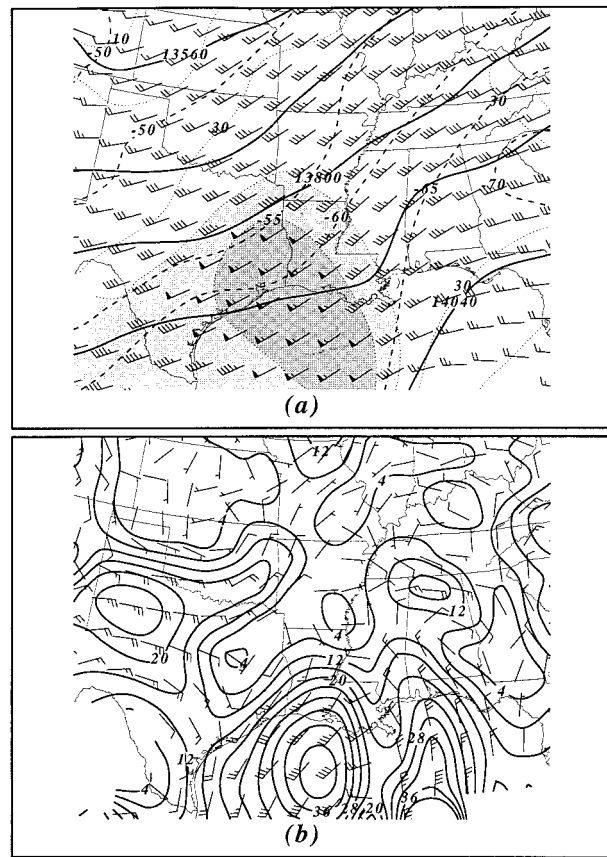FIG. 6. Same as Figs. 2a,b but valid at 0000 UTC 28 March 1994.

FIG. 7. Same as Figs. 3a,b but valid at 0000 UTC 28 March 1994.

into a new dynamical model and clarify the differences between this new theory and the UJ79 paradigm.

2. Numerical simulation experiment

The numerical model employed for the mesoscale numerical simulation experiments is the Mesoscale Atmospheric Simulation System (MASS) (Kaplan et al. 1982; Kaplan and Karyampudi 1992a,b; MESO 1995; Kaplan et al. 1995; Kaplan et al. 1996; Kaplan et al. 1997; Manobianco et al. 1996; Bauman et al. 1997). The hydrostatic model characteristics are described in Table 1. The numerical model employs a Blackadar high-resolution planetary boundary layer and explicit microphysics formulation. The numerical experiment involves both a coarse-mesh and nested-grid fine-mesh full physics simulation integrated over the two matrices, that is, $170 \times 140 \times 30$ coarse-mesh and $200 \times 150 \times 33$ fine-mesh grid points depicted in Fig. 1b. The coarse-mesh ($\sim$24 km) simulation was initialized from conventional rawinsonde and surface datasets at 0000 UTC 27 March 1994 and integrated for 24 h of real time. Additional bogussing was performed to enhance the initial moisture fields based on radar and satellite datasets analogous to Zack et al. (1991). Time-depen-

dent lateral boundary conditions were derived from temporally and spatially interpolated rawinsonde observations. The fine-mesh ($\sim$12 km) simulation was initialized at 0400 UTC and integrated for 20 h of real time. Initial and time-dependent lateral boundary conditions for the fine-mesh simulation were derived from the coarse-mesh simulation. The 12-km horizontal resolution has been employed in conjunction with a convective parameterization scheme and been shown to produce realistic hydrostatic convective ensembles/circulations in many of the above-referenced numerical studies. Since the tornadic activity occurred between 1700 UTC and 2300 UTC 27 March 1994 primarily in Alabama and Georgia, the period of emphasis will focus on 1200 UTC 27 March–0000 UTC 28 March 1994 just upstream over Mississippi and Alabama.

3. Multiple quasigeostrophic jet streak secondary circulations

a. Observations

Figures 2 and 3 depict the 200- and 150-mb NWS observations and analyses as well as the analyzed ageostrophic wind components and **Q**-vector convergence
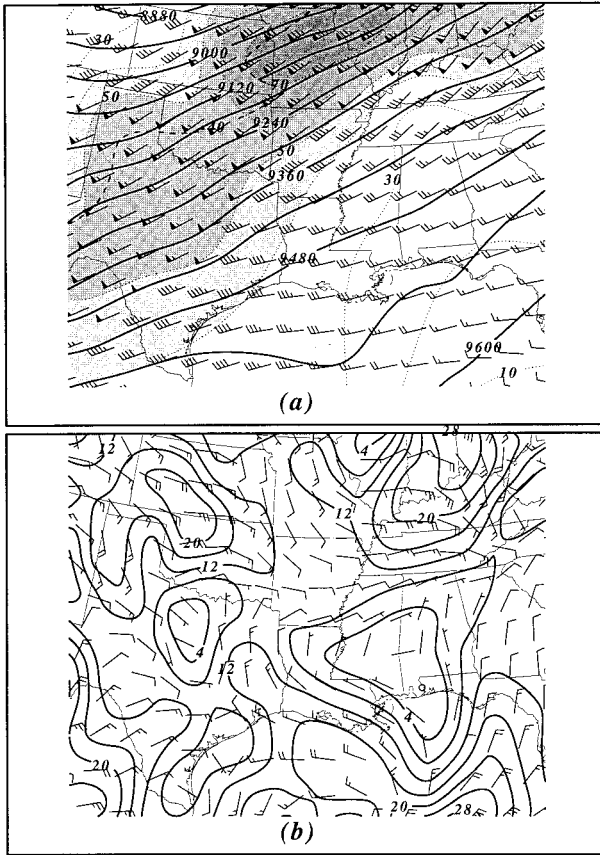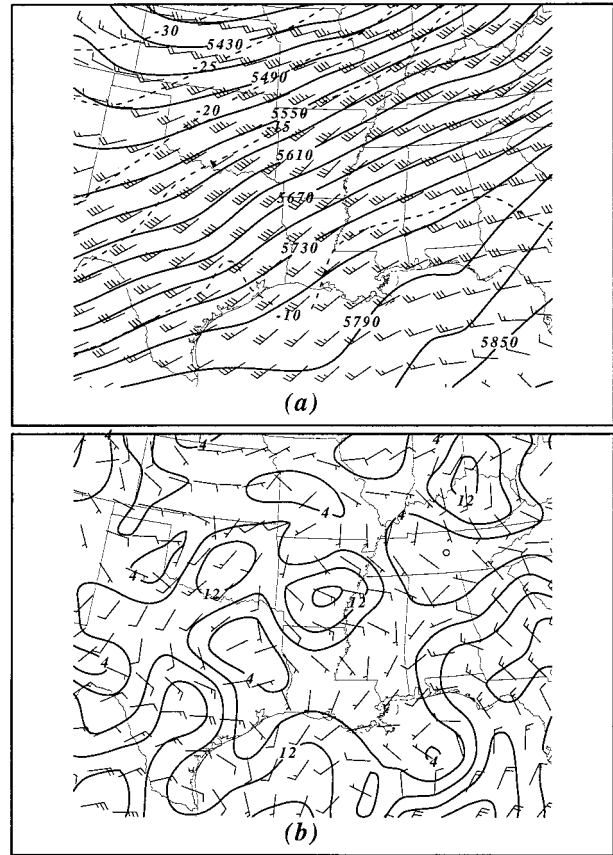
FIG. 8. Same as Figs. 2a,b but for 300 mb.

FIG. 9. Same as Fig. 8 but for 500 mb.

fields over the southeastern and south-central United States all valid at 1200 UTC 27 March. Furthermore, Fig. 8 depicts the 300-mb observed total and ageostrophic wind components at the same time. These figures indicate that at 1200 UTC two jet streaks are evident. The northern jet or polar jet (PJ) is most evident at 200 mb and centered over southern Illinois and a southern jet or subtropical jet (STJ) is, relatively speaking, more evident at 150 and 300 mb. The entrance region of the PJ at 200 mb and its leftward-directed cross-stream ageostrophic flow is best developed over eastern Oklahoma, northeastern Texas, and western Arkansas. The exit region of the STJ can be seen at 300, 200, and 150 mb over eastern Alabama, western Georgia, and the Florida Panhandle extending southward off the Gulf of Mexico coast. The along-stream velocity gradient at 300, 200, and 150 mb within the exit region of the STJ exists over the region from Mississippi to Georgia [note the region in between Jackson, Mississippi (JAN), and Waycross, Georgia (AYS), at 300, 200, and 150 mb in Figs. 2a and 8a] while a reversed gradient of wind velocity exists within the entrance region of the PJ over central Texas [note the region between Longview, Texas (GGG), and Midland, Texas (MAF), in Figs. 2a and 8a]. Thus, the most significant magnitude of both the PJ

entrance region's leftward-directed ageostrophic flow and the STJ exit region's rightward-directed ageostrophic flow within the 300–150-mb layer as diagnosed from Figs. 2b, 3b, and 8b is likely to occur after 1200 UTC over the region in between the Florida Panhandle/southern Georgia and northeastern Texas, that is, northern and central Mississippi and western Alabama. *As will be shown, this region closely follows the observed development and propagation of intense convection some 3–6 h later. Note how portions of this region exhibit a significant signal of quasigeostrophic ascent at 200 and 150 mb as diagnosed from* **Q***-vector convergence fields in Figs. 2c and 3c.* Most of the state of Mississippi exhibits **Q**-vector convergence at 200 and 150 mb in Figs. 2c and 3c, consistent with rightward-directed ageostrophic flow to the southeast over Alabama and the Florida gulf coast depicted in Figs. 2b and 3b.

To diagnose this juxtapositioning of jet streaks at 1200 UTC, the rawinsonde data were employed to calculate transverse ageostrophic circulations relative to the vertical cross section oriented from Cape Girardeau, Missouri (CGI), within the entrance region of the PJ and Pensacola, Florida (PNS), within the exit region of the STJ (note Fig. 1b for location). The middle of the cross section traverses eastern Mississippi and western
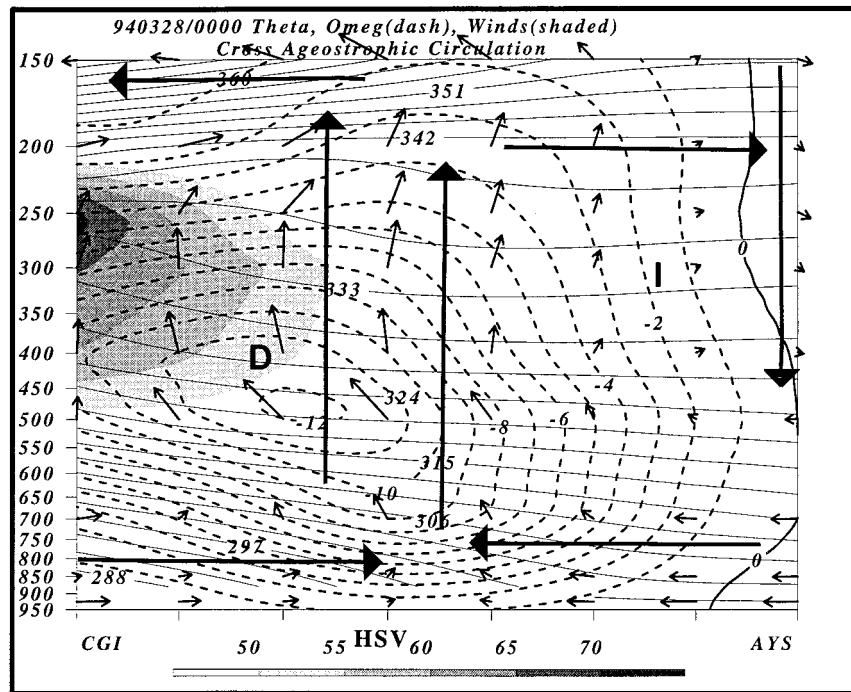
Fig. 10. Same as Fig. 4 but from Cape Girardeau, Missouri (CGI), to Waycross, Georgia (WYS), and valid at 0000 UTC 28 March 1994. See Fig. 1 for location.

Alabama and is centered above Columbus, Mississippi (CBM), the location of the incipient deep convection that develops between 1400 and 1500 UTC affecting eastern Alabama with tornadoes by shortly after 1700 UTC (note Fig. 15). Figure 4 depicts the dual vertical circulations with the following signals: 1) southeastward-directed cross-stream ageostrophic flow above 350 mb south of CBM, 2) northwestward-directed cross-stream ageostrophic flow between CGI and CBM within the 600–300-mb layer, 3) low-level northwestward-directed return branch cross-stream ageostrophic flow directed from PNS to CBM below 850 mb, 4) low-level southeastward-directed return branch cross-stream ageostrophic flow directed from CGI to CBM below 700 mb, and 5) a descending/near zero vertical motion circulation couplet well south of CBM centered near 350 mb and an ascending/descending couplet centered well north of CBM between 700 and 300 mb. The PJ circulation produces ascending vertical motions from 400 mb to the surface while the STJ circulation produces a weakness in descending flow directly above the PJ ascent near where the **Q**-vector computations indicate upward quasigeostrophic vertical motions at 200 and 150 mb, that is, over northern Mississippi. This indicates that *both branches are inducing the deepest ascent and ageostrophic confluent low-level flow as well as ageostrophic diffluent upper-level flow over and/or just south of CBM at 1200 UTC. The arrows in Fig. 4 indicate juxtaposed indirect and direct transverse secondary circulation cells about the STJ and PJ, respectively, consistent with dual transverse balanced secondary circulations. Note, also that the most significant slope in the isentropes occurs over CBM below 700 mb where continental air is located.*

Figures 5a–c depict the 1200 UTC NWS 850- and 700-mb observations and analyses as well as 850-mb **Q**-vector forcing, respectively. Evident are three air masses and two regions of ageostrophic flow. Air of polar origin over the southern plains region [as exemplified by the near 0°C 850-mb temperatures at Amarillo, Texas (AMA), Oklahoma City, Oklahoma (OKC), and Monette, Missouri (MON)] is coming into juxtaposition with maritime tropical air over the southeastern United States and most of the gulf coastal states [as exemplified by the nearly saturated air with near 15°C 850-mb temperatures at Corpus Christi, Texas (CRP), Lake Charles, Louisiana (LCH), Slidell, Louisiana (SIL), and Tallahassee, Florida (TLH)]. The 850-mb dewpoint depressions are very small throughout most of the gulf coastal region; however, hot dry air of Mexican origin is evident over south Texas at Brownsville (BRO) along the Gulf of Mexico coast at both 850 and 700 mb. This continental air is exemplified by the very warm temperatures exceeding 25°C at 850 mb and equaling or exceeding 10°C at 700 mb as well as large dewpoint depressions over the gulf coastal states, for example, at BRO, CRP, and SIL. Thus, the Mexican air is likely being advected from the open waters of the Gulf of Mexico east of BRO in the southwesterly flow above the maritime tropical air along the Gulf of Mexico
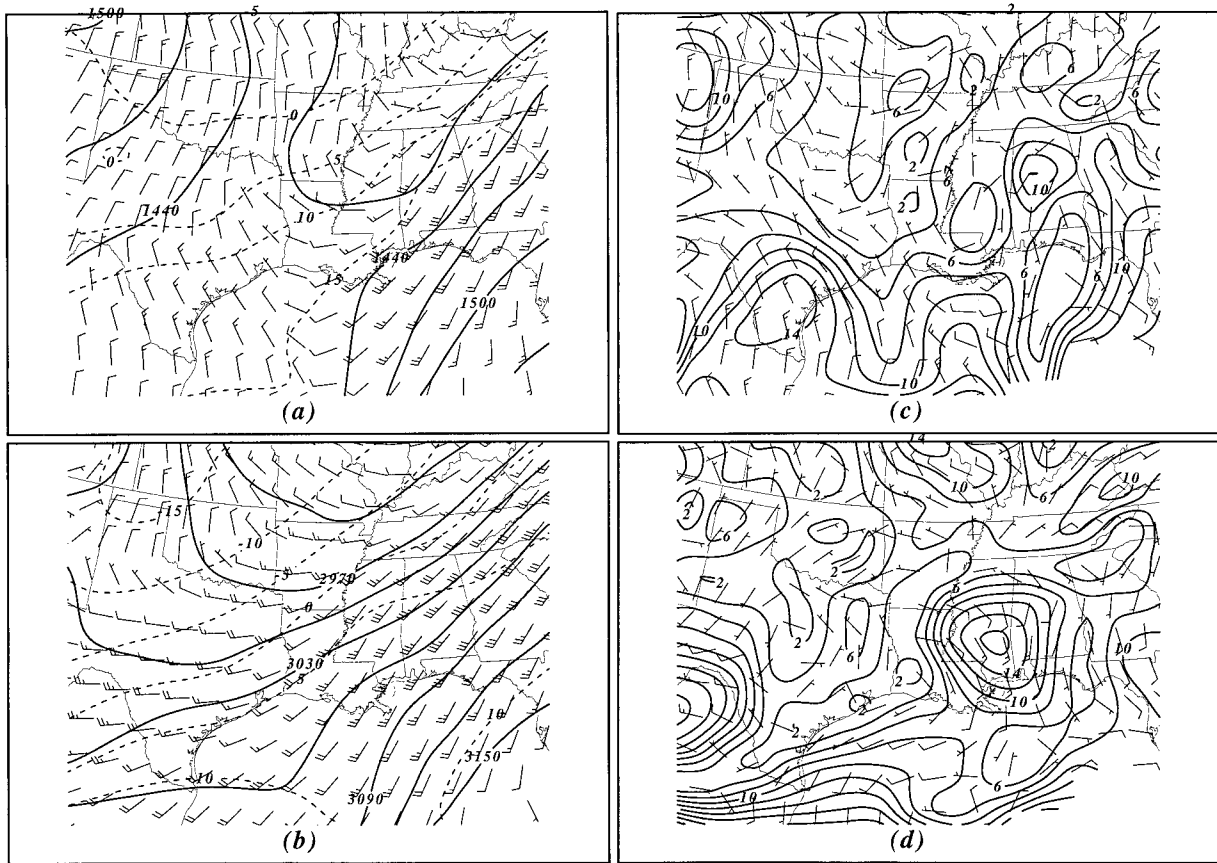
FIG. 11. Same as Figs. 5a,b,d,e but valid at 0000 UTC 28 March 1994.

coastal region. Southerly ageostrophic, that is, leftward-directed, flow is evident along the gulf coast at 850 mb at SIL indicative of the return branch of the STJ transverse ageostrophic secondary circulation (Fig. 5d) while northerly ageostrophic flow is evident behind the cold front at almost every 850-mb station slicing from west Texas through central Tennessee indicative of the low-level ageostrophic return branch under the entrance region of the PJ. Figures 5d,e indicate how the low-level return branch circulation and ageostrophic observations are colocated in space. Figures 4 and 5 clearly show that in between these two low-level return branch circulations quasigeostrophic forcing is producing ascending motion particularly at 850 mb over Mississippi and western Alabama under the ascent depicted in Figs. 2–4. The hot dry air at 700 mb is nearly coincident with the leading edge of southerly ageostrophic flow at 850 and 700 mb implying that the Mexican air is being advected toward the north-northeast above the maritime tropical air as part of the low-level return branch of the STJ's transverse secondary circulation and is coming into proximity with the polar air under the PJ entrance region's transverse secondary circulation over eastern Texas, Louisiana, and Mississippi where **Q**-vector convergence exists (note Fig. 5c). The sloping lower tro-

pospheric isentropic surfaces above and north of CBM depicted in Fig. 4 are signals of this increasing baroclinic structure in between the continental and polar air masses.

By 0000 UTC, as can be seen in Figs. 6a,b and 7a,b, which are the complements of Figs. 2a,b and 3a,b, the split/dual jet structure is quite evident from northeastern Mississippi to western South Carolina. Rightward-directed cross-stream ageostrophic flow is quite evident from CBM to the Florida coastal plain, with an along-stream decrease in wind velocity centered over Alabama, Georgia, and South Carolina at 200 mb, and is shifted somewhat southward at 150 mb. While most of the wind observations at these levels have been blown away within the PJ entrance region, at 300 and 500 mb at both 1200 and 0000 UTC (Figs. 8a and 9a), strong signals of leftward-directed cross-stream ageostrophic flow are evident over northern Mississippi, Alabama, and Georgia (note the analyses in Figs. 8b and 9b). The complement of Fig. 4, that is, Fig. 10, indicates how the dual circulation structure has been replaced largely by a single leftward-directed ageostrophic jetlet that overwhelms the background (larger scale) quasigeostrophic secondary circulations with an ascending vertical motion maximum over northern Alabama and Mis-
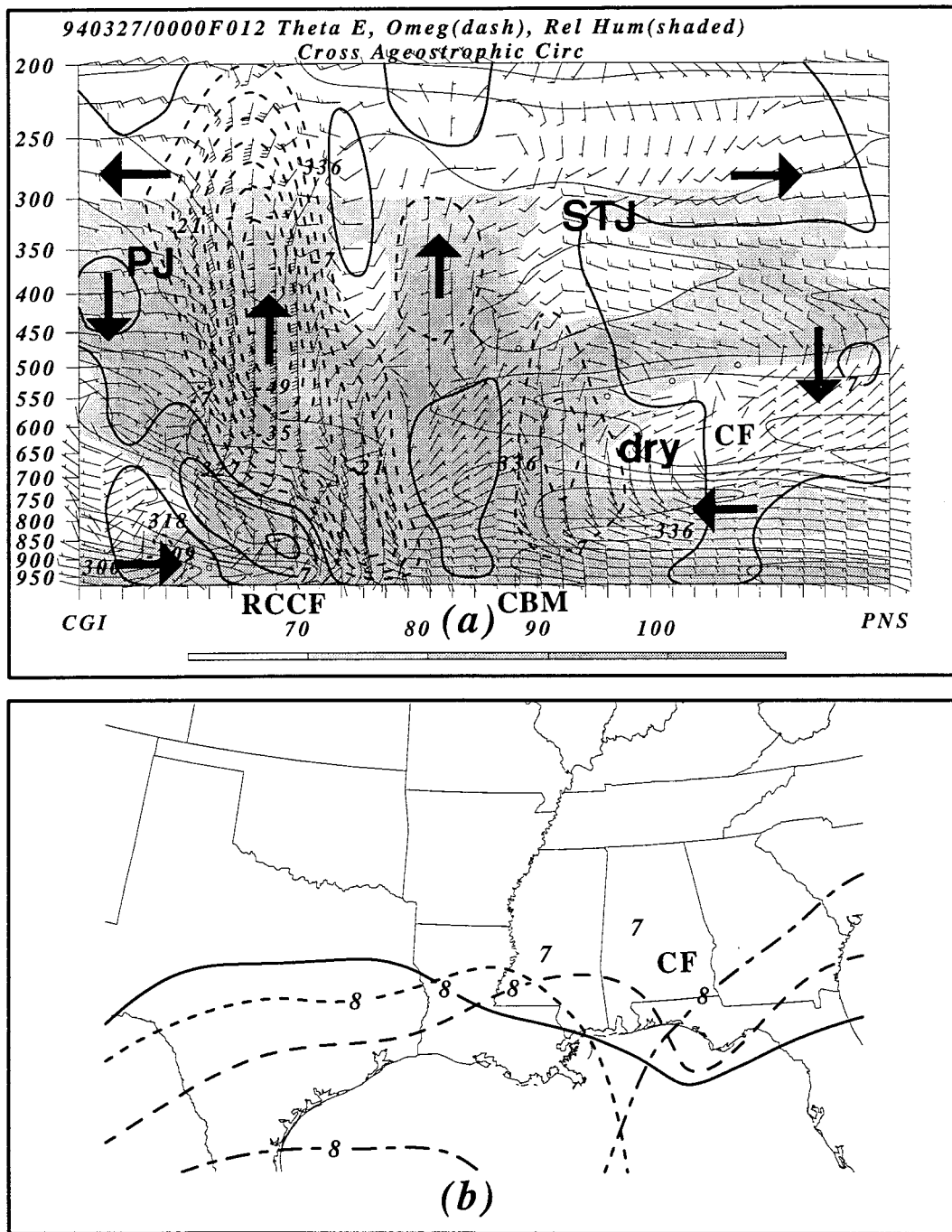
FIG. 12. (a) MASS coarse-mesh simulation vertical cross section from Cape Girardeau, Missouri (CGI), to Pensacola, Florida (PNS), of transverse ageostrophic circulation vectors, omega (dashed upward and thick solid downward in μb s^{-1}), θ_e (thin solid in K), and relative humidity (shaded in percent as depicted on the bottom of the cross section) valid at 1200 UTC 27 March 1994. (b) Observed location of the 700-mb 8°C isoline marking the successive locations of the continental front (CF) at 1200 UTC 26 March (solid), 0000 UTC 27 March (short dashed), 1200 UTC 27 March (long dashed), and 1800 UTC 27 March (short dashed–long dashed) 1994. Observed 700-mb temperatures (7°C) are plotted for the 1800 UTC soundings in Fig. 17. RCCF refers to the rain-cooled cold front.
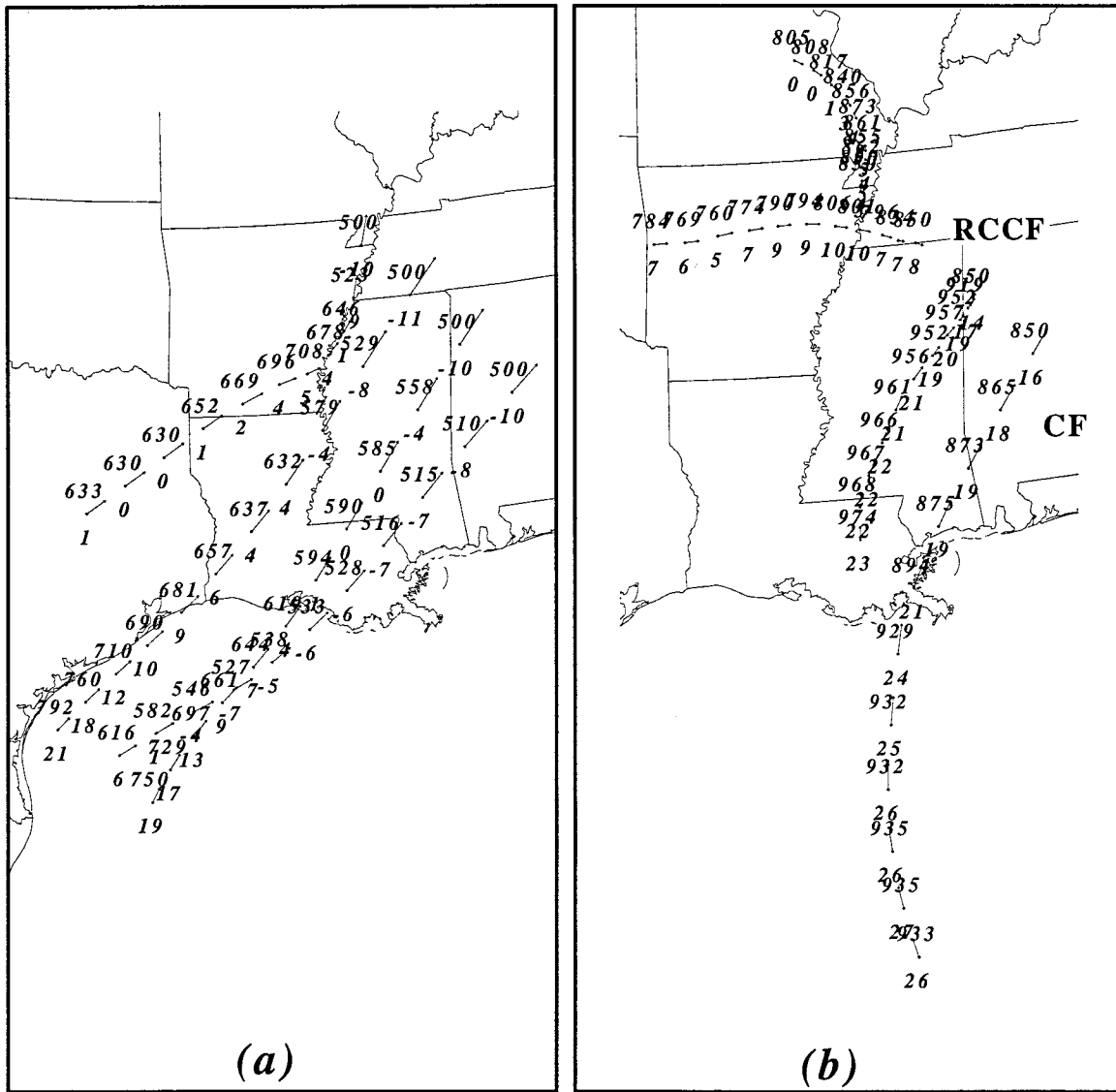
FIG. 13. MASS coarse-mesh simulation backward trajectories beginning at 1700 UTC 27 March 1994 for both the (a) 500- and (b) 850-mb levels. Pressure (mb) and temperature (°C) are depicted at hourly parcel locations. CF and RCCF refer to the continental front and rain-cooled cold front, respectively.

sissippi near 500 mb. At 850 mb, in Figs. 11a,c, the leftward-directed ageostrophic flow accompanying a low-level jet maximum exceeding 25 m s^{-1} is quite evident at Centerville, Alabama (CKL), and Athens, Georgia (AHN), with high temperatures and low dewpoint depressions, while rightward-directed ageostrophic flow can be found from CRP to JAN behind the cold front in the cold moist air indicating the converging low-level jets that may be signals of the return branch circulations of the dual jet streaks and/or additional signals of unbalanced low-level jets. The hot dry air has been restricted to the Florida Panhandle at 850 mb as indicated by large dewpoint depression at TLH while at 700 mb the dry air is largely absent even though it is very warm along the immediate southern Atlantic coastal

plain (Fig. 11b). The leftward-directed and rightward-directed ageostrophic wind components depicted in Fig. 11d are evident above the aforementioned 850-mb features that are consistent with low-level return branch circulations. Thus, even after the tornado outbreak, polar, maritime tropical, and continental air are observed to be still juxtaposed at low levels due, in part, to the ageostrophic return branch circulations accompanying dual jet streaks.

b. Simulations

Figures 12 and 13 depict the substantial areal coverage, depth, and time continuity of the two quasigeostrophic circulations as well as their effects upon the
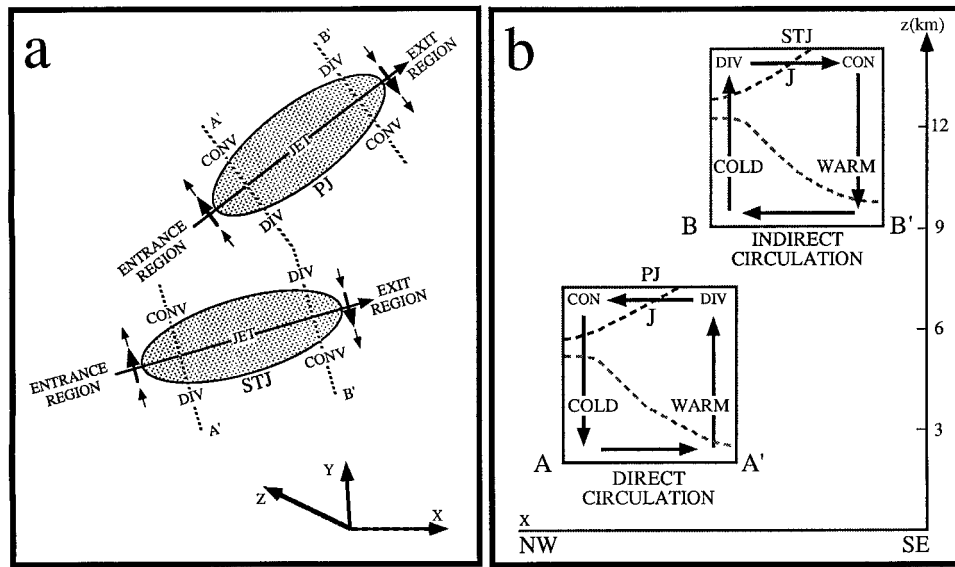
FIG. 14. Schematics depicting (a) horizontal and (b) vertical structures of the transverse ageostrophic circulations about the polar and subtropical jet streaks.

low-level thermal gradients as diagnosed from the coarse-mesh MASS model simulations and observations. The dual transverse circulations, airmass origins, and prolonged transport, as well as the relative locations of the air masses to frontal formation, can be more accurately diagnosed from the much higher resolution structure that is available from the MASS mesoscale model simulation. Figure 12 depicts the dual circulation structure with the added detail in the model indicating that the circulations produce ascent throughout the column above CBM to 200 mb with the exception of the layer between 600 and 800 mb. Just northwest of CBM, a very strong ascent maximum can be found accompanying the low-level circulation above the surface cold front with saturated air. The frontogenetical nature of this circulation is evident as low θ_e air near the surface converges toward high θ_e air accompanying low-level return branch circulations under the PJ and STJ, respectively, analogous to the observations in Fig. 4. The multicellular thermally indirect and thermally direct circulations are rather similar to those observed from rawinsonde data in Fig. 4. The ascent maximum between 550 and 250 mb is sandwiched between the upward branches of the STJ and PJ thermally indirect and thermally direct transverse ageostrophic circulations similar to the observations depicted in Fig. 4. The low-level θ_e minimum surging southeastward is, in part, sustained by precipitation falling into the surface layer resulting in additional evaporational cooling, that is, the rain-cooled cold front (RCCF). Thus the low-level return branch circulation under the PJ entrance region is being enhanced by diabatic cooling. Just south of CBM, between 500 and 800 mb, is a warm and dry layer of air indicative of a secondary elevated θ_e minimum. The flow vectors indicate that this air is being transported

from the southwest between CBM and PNS under the STJ and is drier than the air underneath it. In effect, this warm and dry air enhances the midtropospheric temperature gradient between the PJ and the region southeast of the cold front. Hence, it is located close to the observed dry and warm layer, likely of Mexican origin within the 700–850-mb layer near the Gulf of Mexico coast. In the remainder of the paper the thermal gradient south of the polar front established by the advection of continental air will be referred to as the "continental front" (CF), which is analogous to the "lid edge" in Lanicci and Warner (1991a). Figures 12a,b indicate that this continental front is located just south of CBM as both model and observations (note the 600–700-mb dry wedge in the soundings depicted in Figs. 17a,b) agree on its location during the 1200–1800 UTC time period.

In Fig. 13a we can see that parcels calculated from model-simulated three-dimensional winds, arriving at 500 mb over southeastern Mississippi shortly after 1200 UTC, originated below 600 mb at 0700 UTC just east of CRP. CRP was clearly in the hot dry air of Mexican origin at this time as diagnosed from the 1200 UTC 27 March 700-mb rawinsonde observation at BRO depicted in Fig. 5b as well as the 0000 UTC 27 March rawinsonde observations (not shown). Southeastern Mississippi is the location of the elevated CF near PNS in Figs. 12a,b. Note the extraordinary heat of the parcel originating at 750 mb, with the simulated temperature approaching 20°C at this high elevation (which is close to the average of the observed 1200 UTC temperatures at BRO in Figs. 5a,b)! These parcels are ascending rapidly and turning toward the left as they become part of the low-level return branch of the STJ, while at the same time parcels at 850 mb (Fig. 13b) are located down at 932 mb over
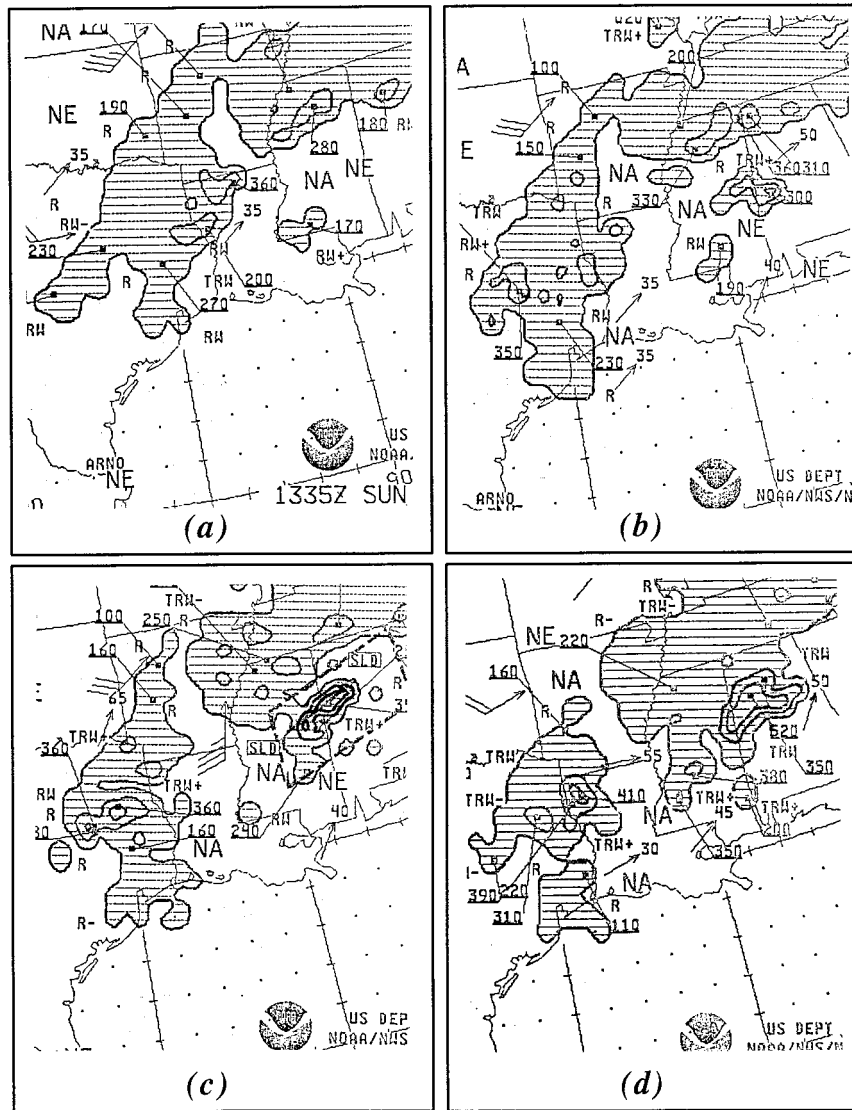
FIG. 15. NWS radar summaries valid at (a) 1335, (b) 1435, (c) 1535, and (d) 1635 UTC 27 March 1994.

the open waters of the Gulf of Mexico, indicative of a probable maritime tropical environment/air mass structure. To substantiate their maritime origin note that these parcels are actually cooler at 870 mb than the parcels originating near CRP were at 750 mb, some ~1200 m higher. Additionally the descent and rightward turning of parcels over Arkansas and northern Louisiana is indicative of the low-level return branch of the PJ. These parcel motions are consistent with the ageostrophic low-level return branch circulations inferred from Figs. 4 and 5d,e. Note that parcels descending behind the cold front over extreme northern Mississippi are cooling, indicative of evaporational cooling effects (overwhelming compressional heating effects) that act to enhance the low-level RCCF boundary depicted in Figs. 12a,b, 13b,

and 16a–d, that is, the boundary between the continental front and polar front. All of these parcels originate well in excess of 500 km away from CBM during the 8-h period prior to the first violent weather over central Alabama. This indicates the large scale of the circulations affecting this region prior to the severe weather.

c. Summary

The simulated and observed transverse circulations and trajectories paint the following mosaic of the atmosphere above CBM prior to the development of the convection that eventually produced the initial Palm Sunday tornadoes. Two large-scale circulations were affecting the transport of parcels into the region above
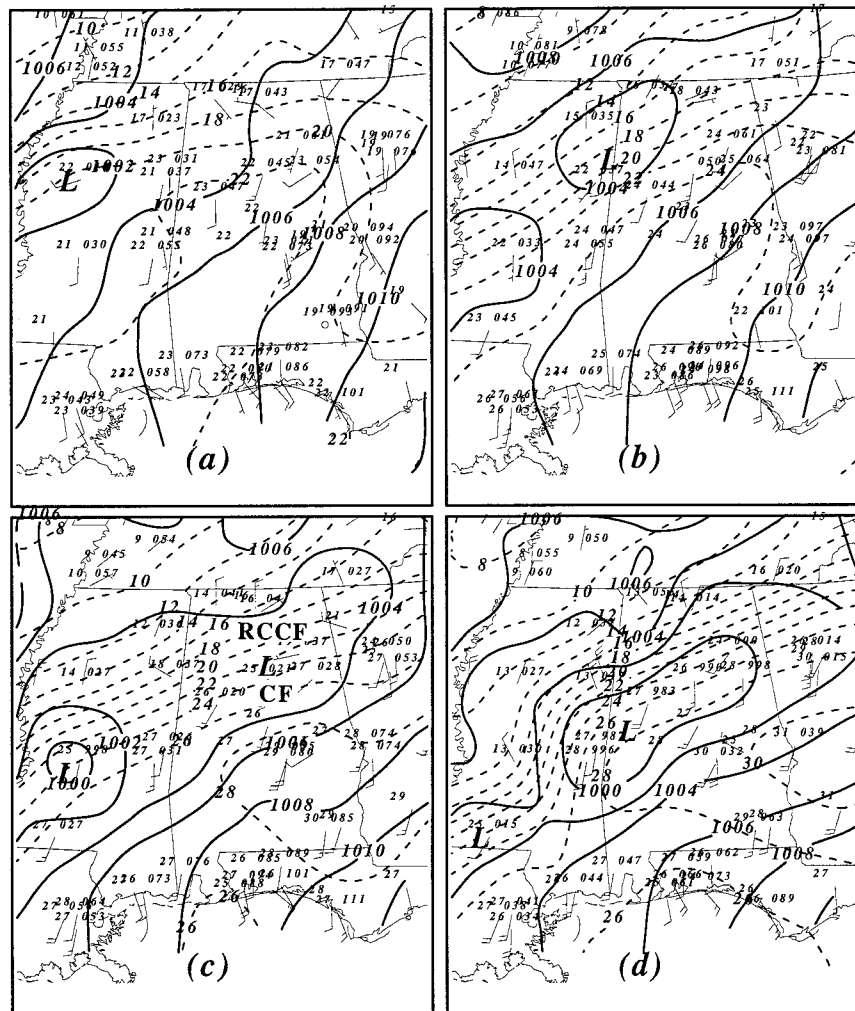
FIG. 16. Surface observation-derived analyses valid at (a) 1200, (b) 1500, (c) 1800, and (d) 2100 UTC 27 March 1994. Sea level pressure is solid lines in mb, surface temperature is dashed in °C, and station winds in knots are plotted.

CBM on or about 1200 UTC over a region of at least 500×500 km if not much larger. Ascent throughout most of the column resulted from the juxtaposed low-level return branches of the PJ and STJ. Air parcels, which originated from both the Gulf of Mexico and near the Texas–Mexico border region 6–12 h earlier, were being lifted under the STJ. The transport under the STJ exit region resulted in the development of warm dry air over warm moist air as well as a secondary mid–lower-tropospheric front south of the polar front and PJ secondary circulation. The juxtapositioning of the PJ transverse entrance region circulation enhanced the deep ascent, producing a diabatically modified surface front accompanying cold advection and precipitation, both of which produced a very sharp low-level θ_e boundary. All of these processes are driven by deep prolonged quasigeostrophic circulation cells. Figure 14 depicts schematically, in a vertical and horizontal plain, the PJ–STJ

circulation structures and coupled physical processes diagnosed from both observations and model output in the previous section. *The ultimate consequence of these dynamics is the increase in the mid–lower-tropospheric northwestward-directed pressure gradient force. This increase in northwestward-directed pressure gradient force accompanies the lower tropospheric frontogenesis across Mississippi shortly before the tornadic convection develops over Alabama at 1730 UTC 27 March 1994.*

4. Deep subgeostrophy and unbalanced jetlet formation southeast of the surface cold front

a. Observations

Figures 15–19 depict key observed fields that span the time period between 1200 UTC 27 March and 0000

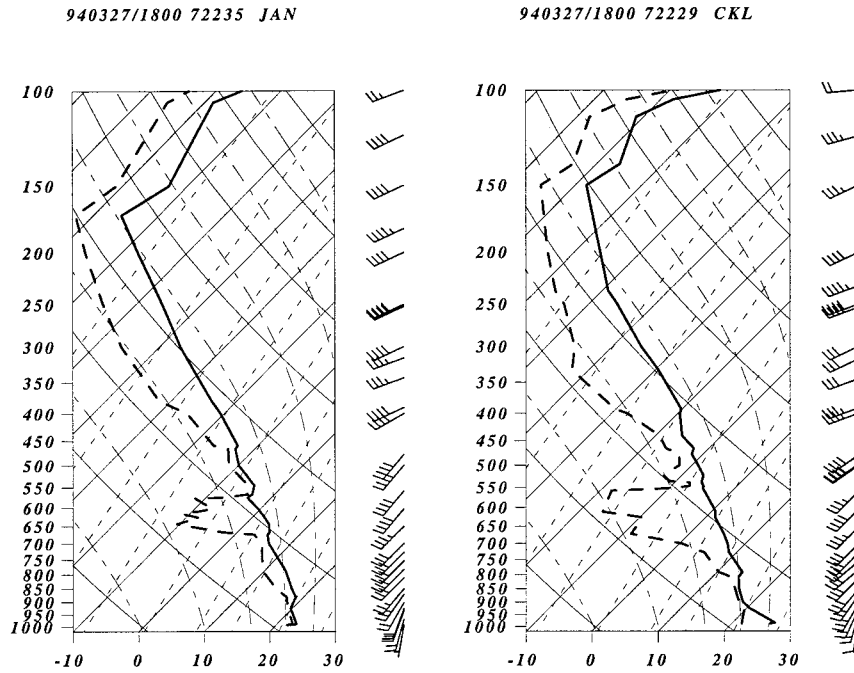940327/1800 72235 JAN   940327/1800 72229 CKL

FIG. 17. Observed soundings at (a) Jackson, Mississippi (JAN), and (b) Centreville, Alabama (CKL), valid at 1800 UTC 27 March 1994. Winds in m s^{-1}.

UTC 28 March 1994. This is roughly 6 h before and 6 h after the first major tornado that affected northeastern Alabama shortly before 1800 UTC. These fields collectively indicate that the region bounded on the north by Huntsville, Alabama (HSV), on the west by JAN, on the south by Montgomery, Alabama (MGM/XMR), and on the east by Atlanta, Georgia (ATL), or roughly centered on CKL represented a region of mid–lower-tropospheric warming and significant mid–lowertropo-
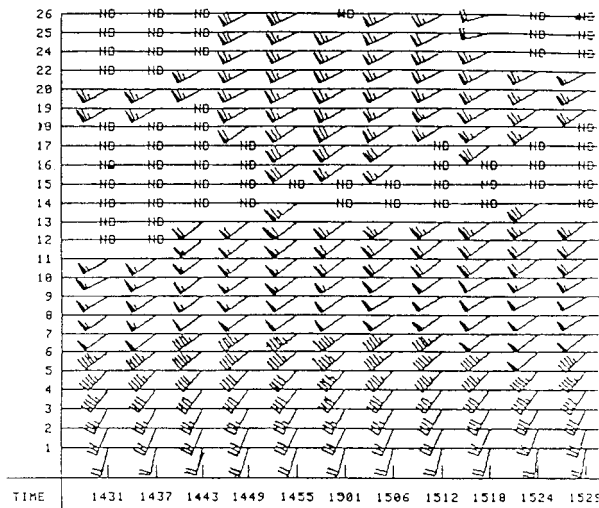

FIG. 18. Observed wind profiles (triangle = 25 m s^{-1} and long barb = 5 m s^{-1}) derived from the MGM/XMR profiler valid from 1431 to 1529 UTC 27 March 1994 (Hales and Vescio 1996).
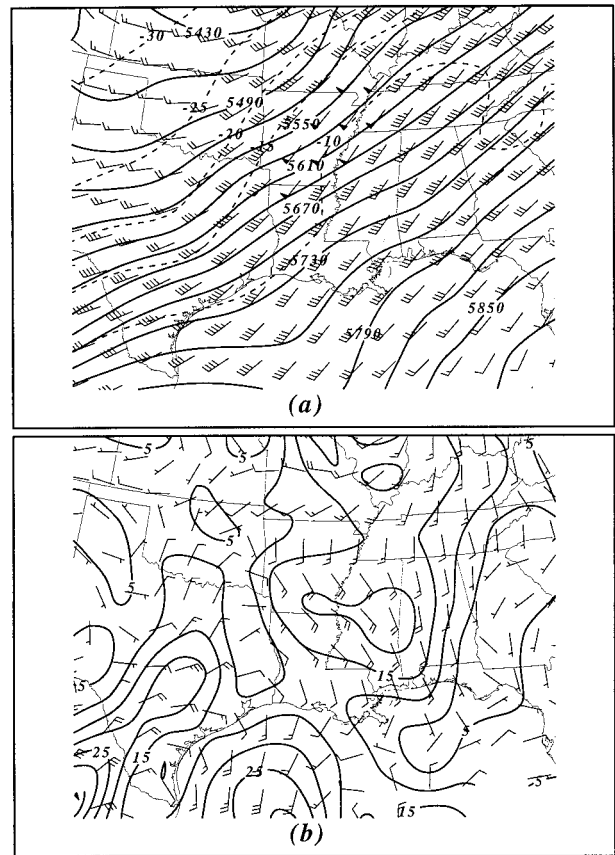

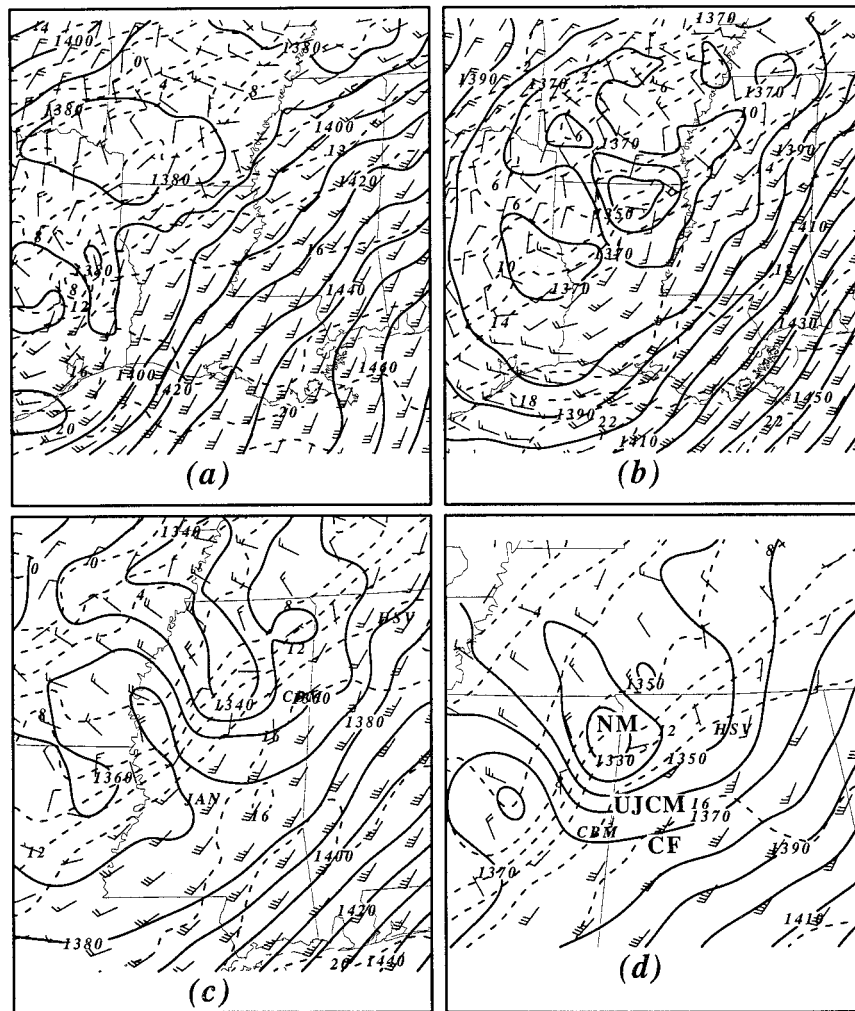FIG. 19. Same as Fig. 9 but valid at 0000 UTC 28 March 1994.

FIG. 20. MASS fine-mesh simulation 850-mb wind barbs (triangle = 50 m s^{-1} and long barb = 10 m s^{-1}), height (solid in m), and temperature (dashed in °C) valid at (a) 1200, (b) 1500, (c) 1700, and (d) 1800 UTC 27 March 1994. CF, UJCM, and NM refer to the continental front, unbalanced jetlet convergence maximum, and northern mesolow, respectively.

spheric accelerations shortly before and nearly coincident with the eruption of violent convection. In Figs. 15a,b can be seen the development of a separate area of convection near CBM shortly before 1500 UTC that becomes severe by 1635 UTC (note Figs. 15c,d). This mesoscale convective system (MCS) rapidly intensifies and propagates eastward across the region between HSV and MGM/XMR just south of the west–east-oriented surface cold boundary depicted in Figs. 16a–d. This MCS, depicted in Figs. 15b–d, is clearly a separate feature from the much shallower convection to the north of the cold boundary near HSV along the Alabama–Tennessee border region (Langmaid et al. 1996). The magnitude of the cross-stream temperature gradient across the west–east boundary between HSV and MGM/XMR increases orthogonal to the path of the MCS during the 1200–2100 UTC period as can be seen depicted in Figs. 16a–d. The increase of surface temperature at

MGM/XMR in the surface southerly ageostrophic flow regime (+7°C) is considerably larger than the decrease of surface temperature at HSV in the surface northerly ageostrophic flow regime (−3°C). The combination results in an increase of surface cross-stream frontal intensity between MGM/XMR and HSV from ∼6°C (200 km)$^{-1}$ to ∼16°C (200 km)$^{-1}$ or an increase of ∼167% in 9 h. This frontogenesis is due, in large part, to ageostrophic confluence where the northerly cross-isobaric flow at HSV is juxtaposed by southerly cross-isobaric flow at MGM/XMR. Said surface frontogenesis has been calculated by Langmaid et al. (1996), who found it to be largely the result of ageostrophic confluence. *However, the frontogenesis is also coincident with the* **Q***-vector ascent diagnosed from Fig. 5c at 1200 UTC. Thus, the frontogenesis is likely the result of diabatically modified quasigeostrophic forcing accompanying the juxtaposed ageostrophic low-level return branch cir-*
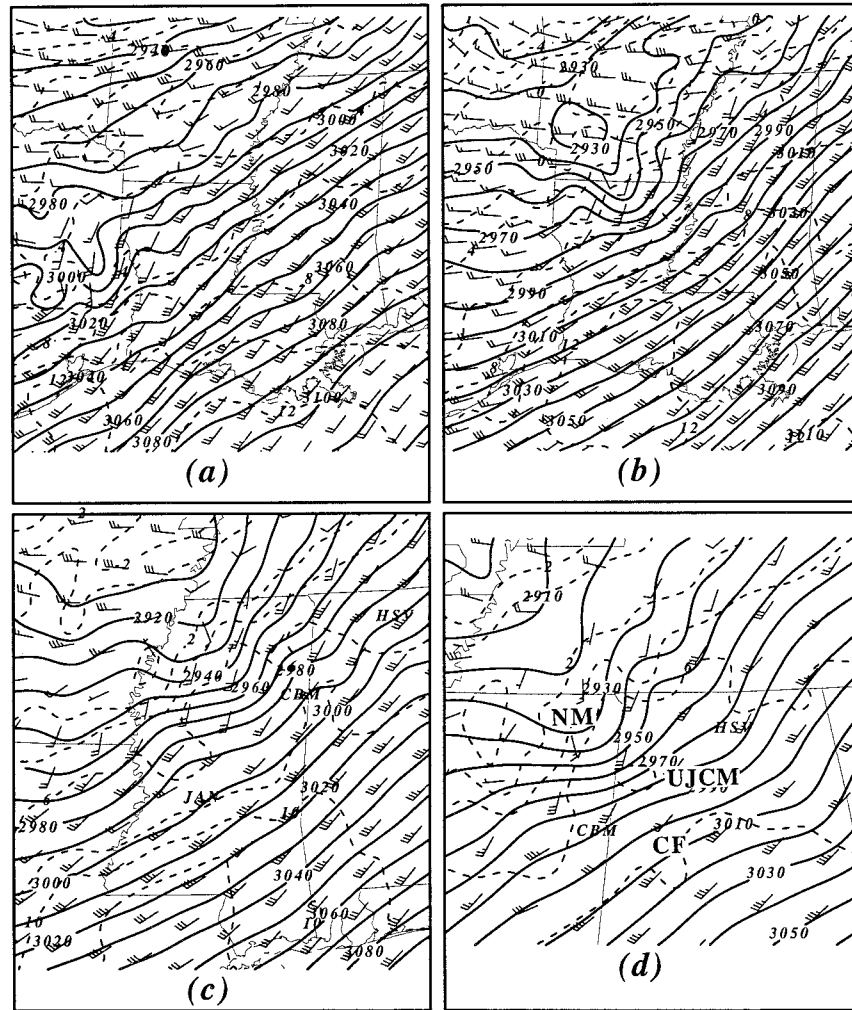
FIG. 21. Same as Fig. 20 but for 700 mb.

culations under the PJ and STJ during its incipient stages, that is, from 1200 to 1500 UTC, or prior to convective development. Furthermore, this surface frontogenesis is occurring just below the region where the MASS model indicated the northeastward transport of hot Mexican air depicted in Figs. 12 and 13 into southern Mississippi and southwestern Alabama by 1200 UTC. Specifically, Fig. 12b depicts the progression of hot dry 700-mb air with temperatures ~8°C, that is, potential temperatures ~310 K, during the 30-h period preceding 1800 UTC. Evident is the warm dry tongue approaching CKL as diagnosed from the special soundings depicted in Figs. 17a,b at CKL and JAN (Hales and Vescio 1996). This hot dry air pool is nearly coincident with the 7°–11°C surface temperature increase during the 1200–2100 UTC period over central and eastern Alabama, that is, at MGM/XMR, or <100 km south of the region of tornadic thunderstorms, that is, the severe weather accompanying the MCS depicted in Figs. 15b–d. The combination of the 700-mb warm dry air-

mass signal, extraordinary late March surface heating with surface temperatures exceeding 30°C, and motion of the MCS all indicate the likelihood that the devastating weather is occurring along a west–southwest- to east–northeast-oriented boundary somewhat, that is, ~50–100 km, south of the surface cold air boundary over northern Alabama and Georgia near HSV.

Figures 17 and 18 unambiguously indicate that the region between JAN, CKL, HSV, and MGM/XMR, within this area of surface heating, is also a region of extraordinary accelerating flow within the midtroposphere during the 1200–1800 UTC time period or roughly coincident with MCS development and low-level temperature increases. Note how the wind velocity at the two sounding locations depicted in Figs. 17a,b have increased from their 1200 UTC values *within the 500–700-mb layer only; that is, upper-level, 400–200-mb winds actually decrease slightly during this 6-h period. This increase indicates that a secondary wind maximum has formed below 400 mb* (Hales and Vescio

1996). Furthermore, the profiler at MGM/XMR depicted in Fig. 18 shows this increase starting at about 1500 UTC or the time of the development of the MCS just to the south of nearby CBM. This secondary wind maximum is occurring almost exactly coincident with the dry wedge in the soundings at CKL and JAN (Hales and Vescio 1996) at 700 mb, indicative of continental air. The location of the increasing flow at 500 and 700 mb is sustained through 0000 UTC as can be inferred from Figs. 10, 11b, 11d, and 19a–b, which indicates a leftward-directed ageostrophic flow at CKL with an extraordinary magnitude at 500 mb, in particular, of ~45 m s^{-1}. These wind observations offer proof that a secondary wind maximum has developed just south of the MCS over central Alabama before 1800 UTC. The wind maximum dominates the flow within the middle troposphere. Also, its orientation has a sufficiently large southerly component to force it to cross the larger-scale isoheights within the midtroposphere directed to the left of the background stream under the exit region of the STJ. It is clearly positioned closer to the STJ exit region over Alabama and Georgia than it is positioned relative to the PJ entrance region over northeastern Texas, Arkansas, and western Tennessee at this time. It is also clearly in proximity to the transport of very warm air northward within the lower troposphere. It is likely, therefore, that this wind maximum is neither associated directly with the PJ, as it is too far to the south, nor is it associated directly with the STJ as it is too low; furthermore, it is too high in altitude to be a low-level jet that is coupled directly to the secondary transverse circulations about either the STJ or PJ. *It is located within the 400–700-mb layer between the upper and lower branches of the transverse secondary circulations.* We will investigate its origins with nested-grid simulation datasets in the next section.

b. Simulations

To understand the mechanism for the intensification of the midtropospheric jetlet, which is observed in proximity to the severe weather and 700-mb surface warming over Alabama and Georgia on and after 1800 UTC, one must diagnose the relationship between the mass and momentum field in proximity to the continental front along the Gulf of Mexico coastal region several hours earlier. First, however, in order to establish the credibility of the nested-grid simulation, which was initialized at 0400 UTC, we will briefly compare the critically important simulated low-level thermal structure to 850- and 700-mb rawinsonde observations depicted in Figs. 5a and 5b, respectively, along the gulf coast. Note that, at 1200 UTC, observed temperatures at 850 and 700 mb indicate a warm air tongue with values ~17° and 8°C, respectively, located from the northernmost Texas gulf coast to southeastern Mississippi. This warm tongue is coincident with relatively dry air at 700 mb that overlays very moist air at 850 mb. Figures 20 and

21 depict nested-grid simulated 850- and 700-mb temperature, winds, and height values at 1200 UTC. A comparison indicates that at 1200 UTC the fields closely mimic the rawinsonde observations of a warm tongue of air from east Texas to southern Mississippi. Most impressive is that the model is able to replicate the northward movement of the 8°C ($\theta = 310$ K) isotherm at 700 mb to an east–west line between Lufkin, Texas (LUF), and Laurel, Mississippi (LUL), which is nearly coincident with the location of the CF depicted in Fig. 12b. One can also see in Fig. 22, which depicts a 1100 UTC cross section normal to the deep air stream from near Stephenville, Texas (SEP), to near Houston, Texas (HOU), that the warm pool at 850 and 700 mb is a reflection of a three-dimensional (continental) frontal zone (CF) displaced to the southeast of the larger-scale frontal zone supporting the PJ entrance region over northeastern Texas at 1200 UTC. This warm pool is inferred from the downfolded lower tropospheric isentropic surfaces northeast of HOU just south of the strong ascending flow. Also evident in Fig. 22 is that there is a secondary 500-mb jetlet simulated to be in proximity to the coastal warm air tongue as diagnosed from the downfolded isentropes just northeast of HOU at 1200 UTC. These two features, that is, the southward-displaced warm front and the secondary 500-mb jetlet are simulated analogs to the observations depicted in the previous subsection. As is shown in Hamilton et al. (1998) this jetlet results from the interaction of the convection and the continental front prior to 1100 UTC.

To examine this interaction and the proceeding geostrophic adjustment process leading to jetlet formation, two trajectories initialized at the center of the coarse simulated 500-mb jetlet have been computed (Table 2). Figures 22c,d reveal the simulated latent heat release and isotachs at the time of trajectory initialization. The acceleration of the parcels in the vicinity of the 500-mb jetlet occur during a time when the pressure gradient force tendency undergoes marked amplification and begins to dominate the force balance acting upon the parcel. This is reflected in the examination of the total acceleration and pressure gradient force values for the two selected parcels. Parcel 1 was chosen at the time just prior to the initial detection of the simulated 500-mb jetlet. The parcel accelerates at the modest rate between 0700 and 1000 UTC, then develops an increasingly large cross-stream ageostrophic component, and accelerates rapidly to the speed of 42 m s^{-1}. A predominant pressure gradient force ($\sim 10^{-3}$ m s^{-2}), and an assisting increase in centripetal acceleration, aids in both the extreme increase in ageostrophic wind magnitude and leftward turning of parcel 1. After 1000 UTC the parcel becomes supergeostrophic and begins to decelerate. Parcel 2 undergoes a similar adjustment but experiences a larger acceleration from 1100 to 1200 UTC. The parcel becomes exposed to an increasingly large cross-stream ageostrophic component and reaches a maximum velocity of 54 m s^{-1} by 1300 UTC.
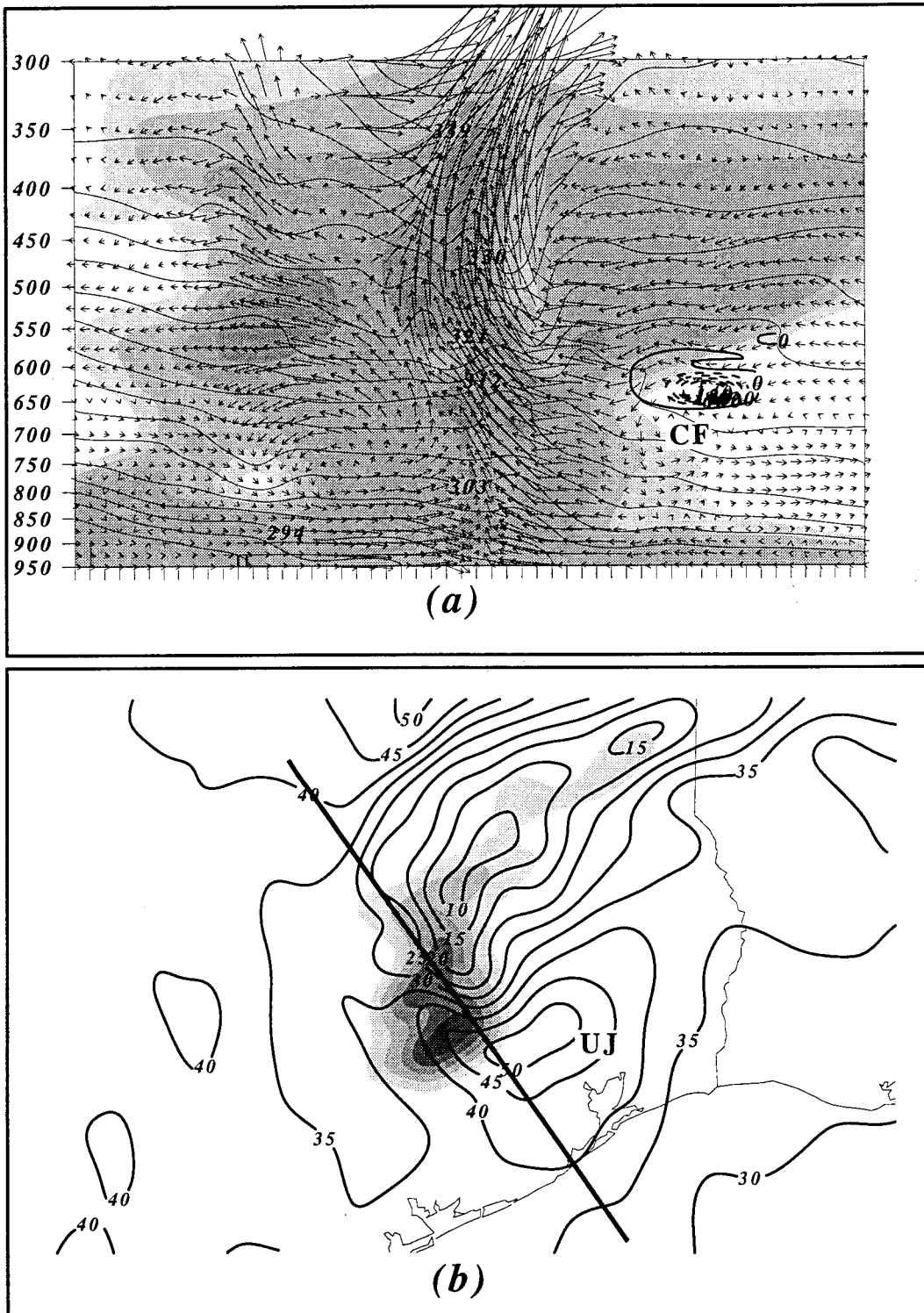
FIG. 22. (a) MASS fine-mesh simulation vertical cross section depicted in Fig. 22b of potential temperature (solid in K), three-dimensional transverse ageostrophic wind vectors, and Richardson number (plotted thick solid and dashed less than 0.25) valid at 1100 UTC 27 March 1994. Here CF is the continental front. (b) MASS fine-mesh simulation 500-mb total wind isotachs (m s^{-1}) valid at 1100 UTC 27 March 1994. Shaded hourly precipitation in mm every 10 mm beginning at 10 mm. Here UJ is the unbalanced jetlet. (c) 1000 and (d) 1100 UTC parcel trajectories initialized at the center of the 500-mb jetlet on 27 March 1994. Trajectories are plotted same as in Fig. 13 with the exception that wind velocities (m s^{-1}) replace temperatures for every hour starting at (c) 0700 and (d) 0800 UTC. Here UJ is the unbalanced jetlet.
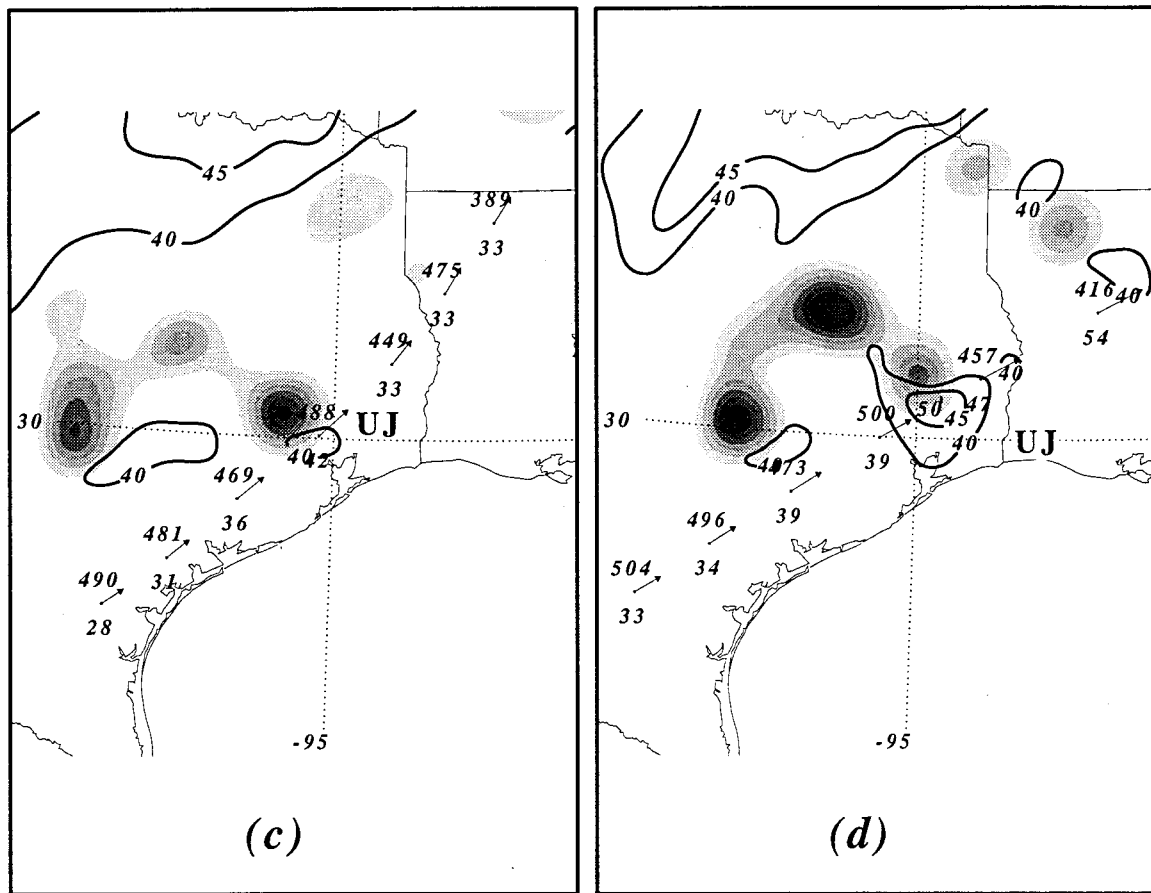
FIG. 22. *(Continued)*

Figures 20–22 indicate how air transported northeastward from south Texas and the Mexican plateau form a secondary (continental) frontal system under and to the southeast of the polar front baroclinic zone, which aids in the maintenance of the jetlet that develops near HOU at 1100 UTC. This secondary front is simulated to rapidly propagate from near the Lousiana–Texas border region southeast of LUF at 1200 UTC to north-central Alabama near CKL at 1800 UTC. The front can be seen to form at 850 and 700 mb to the southeast of

TABLE 2. Data tabulation for parcel trajectories 1 and 2 (Figs. 22c,d) computed through the 500-mb jetlet center from (a) 0700 to 1300 UTC and (b) 0800 to 1300 UTC 27 March 1994. Trajectories are initialized at 1000 (parcel 1) and 1100 (parcel 2) UTC and calculated forward and backward in time. Pressure gradient force (PGF), Coriolis (Co), centripetal (Ce), and tangential (Ta) accelerations are all $\times 10^{-4}$.

Time (UTC)	Pres (mb)	Total accel. Dir. (deg)	mag. (m s^{-2})	PGF ($\times 10^{-4}$) Dir. (deg)	mag. (m s^{-2})	Co accel Dir. (deg)	mag. (m s^{-2})	Ce accel. Dir. (deg)	mag. (m s^{-2})	Ta accel. Dir. (deg)	mag. (m s^{-2})
Parcel 1											
0800	481	204	3.09	177	4.42	318	2.16	138	1.25	228	2.82
0900	469	237	1.42	168	2.67	317	2.54	137	0.26	227	1.40
1000	488	148	8.78	145	11.76	316	3.03	136	8.59	226	1.84
1100	449	66	4.32	87	5.88	308	2.46	128	2.01	218	3.82
1200	475	161	3.09	143	2.52	301	2.52	121	2.39	211	1.96
Parcel 2											
0800	504	178	1.26	156	3.36	324	2.24	144	1.04	234	0.71
0900	496	256	1.17	173	2.19	323	2.36	143	0.45	233	1.08
1000	473	267	3.51	218	3.09	325	2.77	145	1.88	235	2.96
1100	500	219	1.11	167	3.37	329	2.84	149	0.37	239	1.05
1200	457	270	5.91	234	5.21	331	3.52	151	2.86	241	5.17

the northernmost mesolow (NM), which sweeps north-eastward from southwest of Greenville, Mississippi (GLH), at 1500 UTC to north of Birmingham, Alabama (BHM), at 1800 UTC. It is this NM in conjunction with the intensifying secondary CF that is the key to the severe weather that soon develops downstream over Alabama. As this secondary frontal system translates east–northeastward, the southeast–northwest height gradient within the troposphere increases across the same region. For example, between JAN and Columbus, Georgia (CSG), the 850-mb height gradient depicted in Fig. 20 increases from ~45 m (500 km)$^{-1}$ to ~75 m (500 km)$^{-1}$ during the 1200–1700 UTC time period. This nearly 67% increase in the cross-stream midtropospheric height gradient reflects the combined effects of 1) the south-eastward movement of the cold front, including the cooling accompanying rain-cooled air (RCCF); 2) the east–northeastward movement of the warm air accompanying the secondary warm pool along the gulf coast, that is, CF; and 3) the release of latent heat as simulated MCSs form within the conditionably unstable air accompanying the downfolded isentropes depicted in Fig. 22 just north of the continental front. Propagating along this height gradient are two 850-mb mesolows positioned at 1200 UTC (note Fig. 20a) just downstream from their observed surface location depicted in Fig. 16a. The most important northern 850-mb mesolow (NM) is located over southern Arkansas near El Dorado (ELD) by 1200 UTC and a second is located over eastern Texas near LUF as can be seen depicted in Fig. 20a. The increasing height gradient southeast of the mesolows, that is, between the cold air over northern Mississippi and the hot air over southeastern Mississippi acts to induce multiple regions of subgeostrophy between these two low-level air pools, that is, between the southeastward-directed cold and rain-cooled PJ low-level return branch and the warm continental air that is caught up in the low-level north-northwesterly directed return branch of the STJ as can be seen in Figs. 23c,d and 24c,d during the 1700–1800 UTC period (note also the simulated trajectories in Fig. 13 to see the confluence of different air masses). During the period between 1500 and 1800 UTC this region of subgeostrophy, caused by the intensifying cross-stream height gradient to the southeast of NM, in particular, propagates from southwestern Louisiana near AEX to northcentral Alabama near HSV and, as it does so, rotates toward the right foreward flank of the 50 m s^{-1} 500-mb jetlet maximum (UJ), thus producing UJS. By 1700 UTC, an unbalanced jetlet convergence maxima (UJCM) can be seen to form in Figs. 20c and 21c ahead of the accelerating 850- and 700-mb jetlets' exit region between JAN and HSV. This lies under the UJS in the right front quadrant of the unbalanced 500-mb jetlet. One region of subgeostrophy located from northeastern Texas through western Tennessee is north of the cold front as diagnosed from the packing of the isotherms and cold advection at 850 mb in Fig. 20. Here, the northwestern periphery of latent heating maxima

extend back over the cold air producing intense regions of subgeostrophy (note Fig. 12a). The secondary southeastward shifted maxima of subgeostrophy (UJS) represents secondary geostrophic wind maxima just north of the continental front, that is, the 8°C 700-mb isotherm where the thermal wind structure of the simulated atmosphere departs from geostrophic balance as a result of the wedging of the continental air at low levels under the deep diffluent circulations between the two jet streaks and just southeast of the rain-cooled cold air (note Figs. 12a and 13b). In effect, the thermal perturbation resulting from the wedging of continental air into the lower troposphere juxtaposed with the southward-propagating RCCF and latent heat release in simulated convection north of the continental front enhances the northwestward-directed low-level pressure gradient force increasing the potential for thermal wind imbalance, particularly if rightward-directed supergeostrophic flow develops aloft. The scale of the UJS (note Figs. 23c,d and 24c,d for the signal of these features to 500 mb between JAN and HSV) and subsequent simulated jetlet is consistent with that of a sub-Rossby radius of deformation (λ_R) circulation as dictated by the following expression from Kaplan et al. (1997):

$$\lambda_R = \frac{NH}{(\zeta + f)^{1/2}(2VR^{-1} + f)^{1/2}}, \tag{1}$$

where N is the Brunt–Väisälä frequency, H is the depth of the subgeostrophic circulation, f is the Coriolis parameter, and ζ is the relative vorticity. Using simulated representative values of these variables over CBM within the simulated convective region at 1700 UTC of $N = 1.15 \times 10^{-3}$ s^{-1}, $H = 9.0 \times 10^{-3}$ m, $f = 7 \times 10^{-5}$ s^{-1}, $VR^{-1} = 1 \times 10^{-4}$ s^{-1}, and $\zeta = -4 \times 10^{-5}$ s^{-1} results in a Rossby radius value of ~300 km. *Since the rotational wind is not the mechanism of adjustment at scales of motion shorter than 300 km, the mass field rather than the wind field adjusts in such an unbalanced flow regime.* As can be seen in Figs. 23c,d and 24c,d, the increasing subgeostrophy is accompanying an increasing leftward-directed ageostrophic jetlet (UJLDA) that develops over eastern Texas near LUF at 1200 UTC and explosively propagates east–northeastward to be over northwestern Alabama between CKL and HSV by 1700 UTC. The simulated increasing winds of >25 m s^{-1} at 850 mb and >35 m s^{-1} at 700 mb depicted in Figs. 20c,d and 21c,d are somewhat stronger and develop sooner than observed in Figs. 17–18; however, their location is consistent with the concept of accelerating mid–lower-tropospheric flow in proximity to the continental front and newly developing MCS between JAN and CKL just before 1800 UTC.

The movement of the simulated leftward-directed ageostrophy (UJLDA) and the simulated subgeostrophy (UJS) regions at 500 mb within the exit region of the UJ can be seen depicted in Figs. 23c,d and
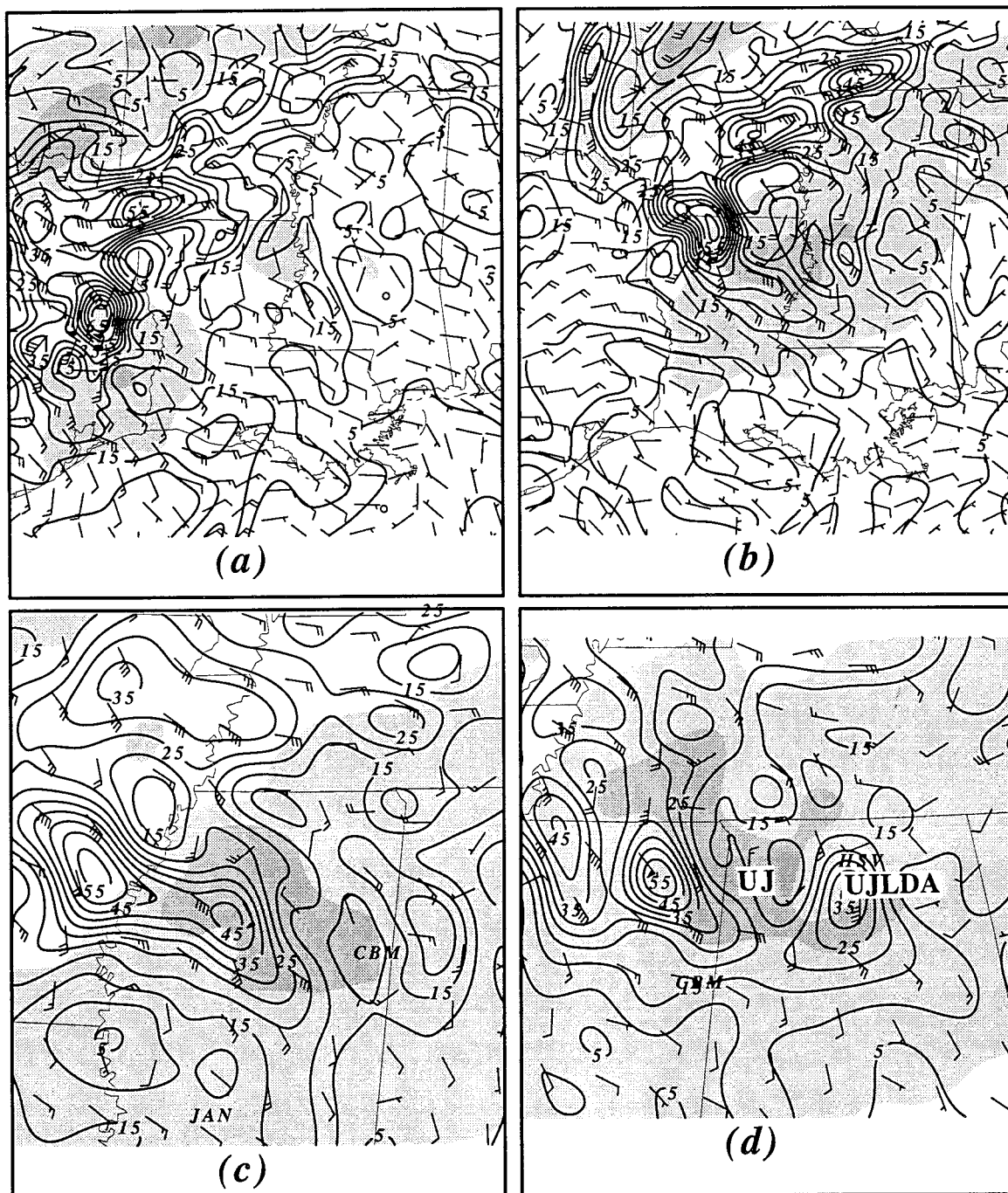
FIG. 23. MASS fine-mesh simulation 500-mb ageostrophic wind barbs (as in Fig. 20) and isotachs (m s^{-1}) valid at (a) 1200, (b) 1500, (c) 1700, and (d) 1800 UTC 27 March 1994. Jetlet at 500 mb is shaded in 10 m s^{-1} intervals beginning at 40 m s^{-1}. Here UJ is the unbalanced jetlet and UJLDA is the unbalanced jetlet leftward-directed ageostrophy.

24c,d, respectively, for the 1700–1800 UTC period. This jetlet, or sub-Rossby radius of deformation jet streak, which develops southeast of the PJ entrance region due to the combined effects of the upstream continental front and its accompanying convection prior to 1200 UTC (Fig. 22), is decidedly unbalanced

in structure. It propagates along the same path of the observed MCS that develops over CBM shortly after 1435 UTC, that is, it moves from northeast of HOU at 1200 UTC, to north-central Louisiana near AEX at 1500 UTC, to northeastern Mississippi near CBM at 1700 UTC, and then into southwestern Tennessee and
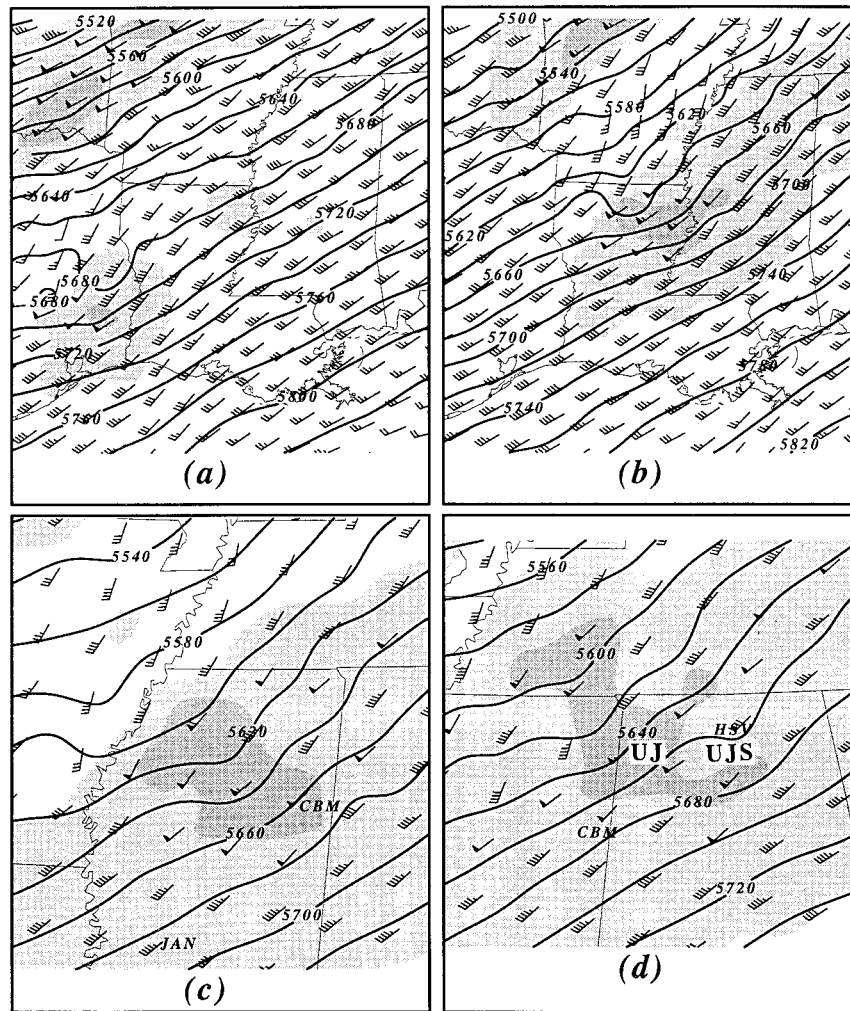
Fig. 24. MASS fine-mesh simulation 500-mb wind barbs (m s⁻¹) and isotachs (as in Fig. 23) and height (solid in m) valid at (a) 1200, (b) 1500, (c) 1700, and (d) 1800 UTC 27 March 1994. Here UJ and UJS are the unbalanced jetlet and unbalanced jetlet subgeostrophy, respectively. MASS fine-mesh simulation 500-mb omega (dashed upward and solid downward in μb s⁻¹) and isotachs (as in Fig. 23) valid at (e) 1200, (f) 1500, (g) 1700, and (h) 1800 UTC 27 March 1994. Here UJ is the unbalanced jetlet and UJRFA is the unbalanced jetlet right forward ascent.

northwestern Alabama west of HSV by 1800 UTC, thus moving at a velocity in excess of 30 m s⁻¹ accompanying the NM depicted in Fig. 20. It is unbalanced because the mass perturbations resulting from the lower tropospheric warm pool as well as simulated latent heating, produce *subgeostrophic (UJS) and leftward-directed accelerating flow (UJLDA) within the right exit region of the jetlet, which is inconsistent with the balanced UJ79 model of a jet streak secondary circulation wherein said flow occurs in the right entrance region. In effect, the jetlet is not in thermal wind balance due to its highly ageostrophic structure resulting from the heating-induced mass perturbation, for example, Kaplan et al. 1997. Ascent and adiabatic cooling (UJRFA and UJRFCP) occur where sinking is supposed to be occurring based on balanced jet streak dynamics* (note Figs. 24h and 28d). This 500-mb leftward-directed ageostrophy, subgeostrophy, ascent, and cooling within the right forward flank of the jetlet can be seen propagating east–northeastward from northeastern Mississippi near CBM at 1700 UTC to northwestern Alabama near HSV by 1800 UTC in Figures 23c,d; 24c,d; 24g,h; and 28c,d as features denoted by the labels UJLDA, UJS, UJRFA, and UJRFCP, respectively. The jetlet is essentially propagating along the northwestern periphery of the warm wedge (lid edge/CF) at 700 mb and the secondary subgeostrophic region formed about this wedge is displaced to the southeast of the subgeostrophy accompanying the PJ entrance region.
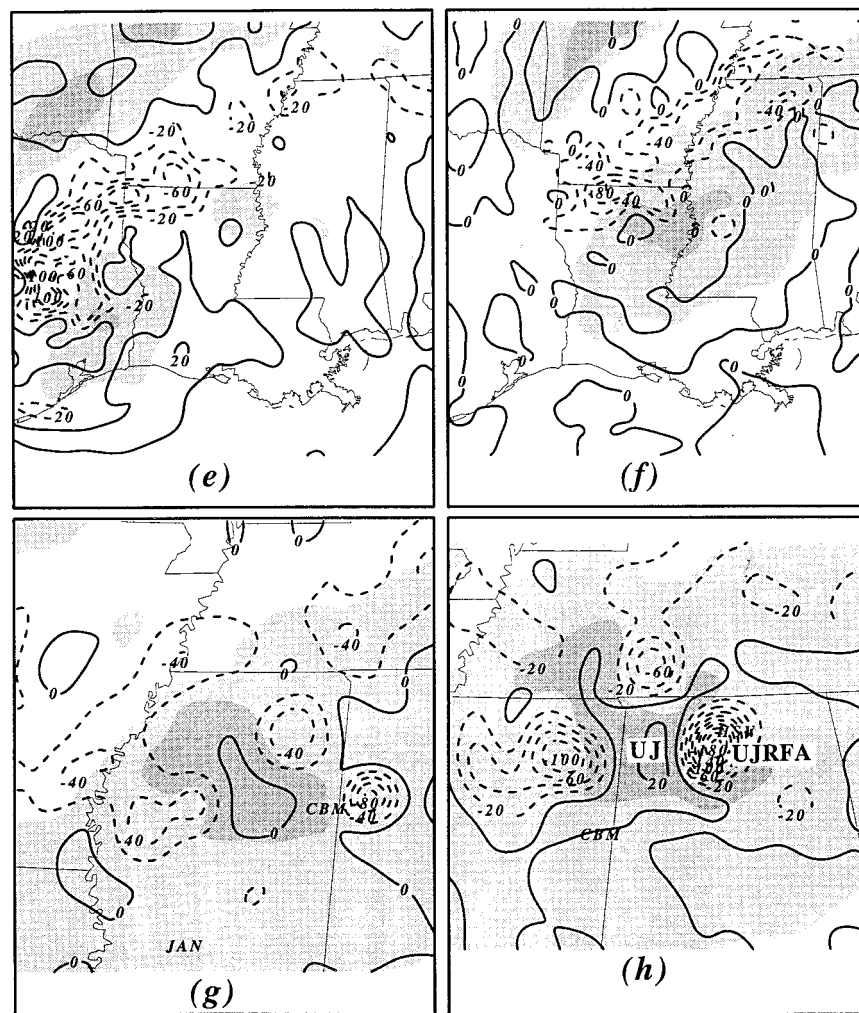
FIG. 24. *(Continued)*

The warm advection at 700 and 850 mb as well as the surface sensible heating (note Figs. 20a,c; 21a,c; and 25a,c over southern Mississippi and Alabama accompanying the NM) act to reinforce the development of the continental front surfaceward. As this occurs the thermal wind imbalance accompanying the southward-shifted ageostrophy is maintained south of the polar front, providing a preferred region for the development and maintenance of the unbalanced jetlet.

By 1700 UTC, the wind velocity at 500 mb increases to ~45 m s^{-1} depicted in Fig. 24c near CKL, which is slightly exceeding the value in the observed CKL sounding depicted in Fig. 17b. The jetlet is a continuously self-generating feature wherein 1) wave–CISK (conditional instability of the second kind) acts to maintain midtropospheric outflow and cooling, 2) the CISK occurs above surface sensible heating, 3) the surface heating occurs ahead of latent heating and midtropospheric warming, which is 4)

above low-level evaporational cooling upstream from the surface sensible heating. The details of how CISK maintains the unbalanced jetlet will be described employing both MASS model and idealized simulations by Hamilton et al. (1998), which is a companion paper in this journal. Figures 25 and 26 indicate, however, that as the first surface mesolow (NM) with its pronounced low-level confluence and along-stream vorticity/inflow structure (UJSC and UJSVM) propagates from northwestern Mississippi near CBM to northeastern Alabama near HSV during the 1700–1800 UTC time period, the midtropospheric jetlet and its right flank cooling (UJRFA) result in the superpositioning of midtropospheric outflow and low-level inflow (UJSC) to the right of the background core of the unbalanced jetlet. The inflow, that is, unbalanced jetlet surface confluence (UJSC in Fig. 25c) accompanying the first mesolow (NM), is obvious from the increasing surface absolute vertical vorticity maxi-
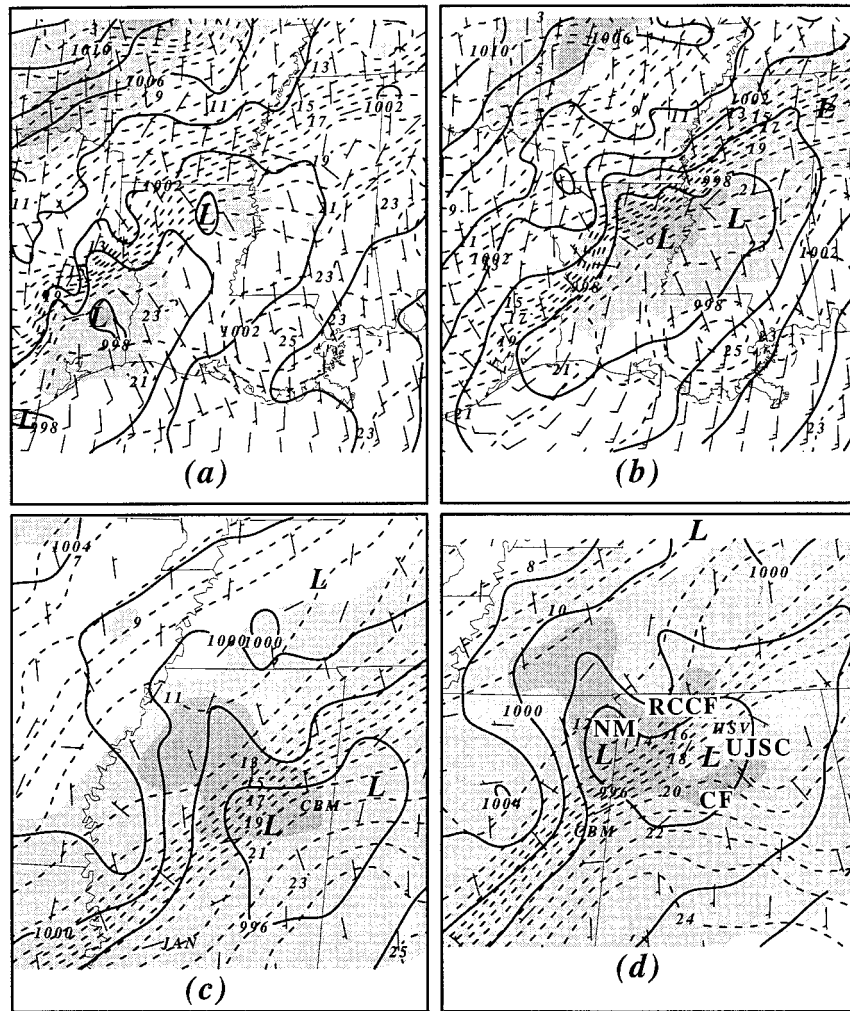
FIG. 25. MASS fine-mesh simulation mean sea level pressure (mb), 2-m wind vectors (as in Fig. 20), and 2-m temperature (°C) and 500-mb isotachs (as in Fig. 23) valid at (a) 1200, (b) 1500, (c) 1700, and (d) 1800 UTC 27 March 1994. UJSC is the unbalanced jetlet surface confluence, NM is the northernmost mesolow, RCCF is the rain-cooled cold front, and CF is the continental front.

mum exceeding 1×10^{-4} s^{-1} (note the unbalanced jetlet surface vertical vorticity maximum that is located near HSV in Fig. 26d). This vertical vorticity maximum is approaching the region of tornadogenesis over northeastern Alabama at 1800 UTC in Fig. 26d to the southeast of the surface rain-cooled cold front (RCCF in Fig. 25d) and to the northeast of the surface warm front (CF in Fig. 25d).

The observed thermally direct circulation producing cooling ahead of the leftward-directed ageostrophic 500-mb flow depicted in Figs. 10 and 19 provide observational evidence for the unbalanced nature of the midtropospheric flow and the downstream cooling accompanying it. Note the structure of the simulated cross section at 1600 UTC depicted in Fig. 27 over the region of the observed intensifying MCS where a region of

intense ascent has formed along the right flank of the jetlet near CBM.

c. Summary

A midtropospheric wind maximum is observed to develop in proximity to the region where severe weather occurs over northcentral Alabama. The nested-grid simulation indicates that the wind maximum is part of a mesoscale jetlet that develops between the exit region of the STJ and entrance region of the PJ. The jetlet is the result of the increasing southeast–northwest-oriented pressure gradient force between the convectively (diabatically) modified low-level return branches of the transverse ageostrophic secondary circulations. The jetlet is unbalanced because sub-
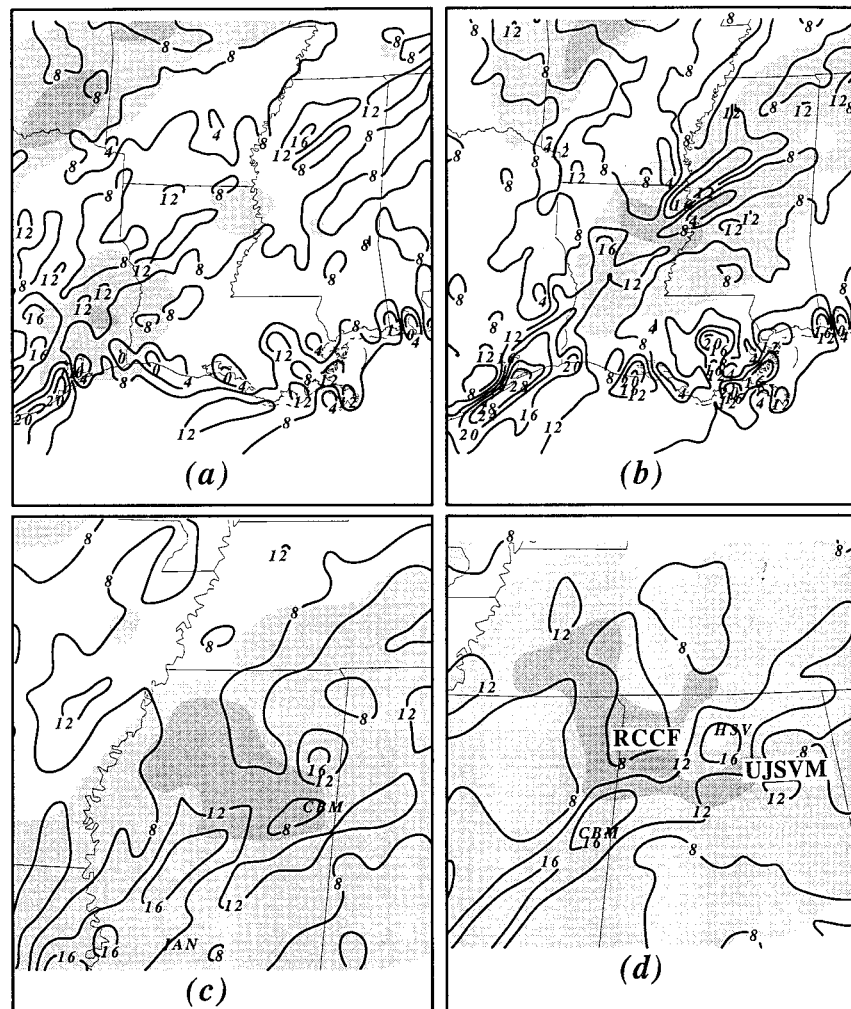
FIG. 26. MASS fine-mesh simulation 2-m absolute vertical vorticity ($s^{-1} \times 10^{-5}$) and 500-mb isotachs (as in Fig. 23) valid at (a) 1200, (b) 1500, (c) 1700, and (d) 1800 UTC 27 March 1994. Here UJ is the unbalanced jetlet, UJSVM is the unbalanced jetlet surface vorticity maximum, RCCF represents the location of the rain-cooled cold front, NM represents the location of the northernmost mesolow, and CF represents the location of the continental front.

geostrophy and ascent are maintained by wave–CISK within the right foreward flank of the jetlet, which enhances right foreward cooling above inflowing planetary boundary layer air. In essence, the jetlet represents the component of a gravity wave that propagates within the conditionally unstable air between the continental and polar fronts and is sustained by wave–CISK.

5. Implications of the unbalanced jetlet for severe weather development

Recently, one of the most widely applied paradigms relating the larger-scale environment to severe storm formation and intensification involves the concept of storm-relative helicity (Davies-Jones 1984). Storm-relative helicity (SRH) is defined by Eq. (2):

$$ \text{SRH} = -\int_0^h \mathbf{k} \cdot (\mathbf{V} - \mathbf{c}) \times \frac{d\mathbf{V}}{dz} \, dz, \qquad (2) $$

wherein the key components are the existence of significant low-level vertical wind ($\mathbf{V}$) shear as well as a significant deviation of storm motion to the right of the mean wind in the column ($\mathbf{c}$). This paradigm is dependent upon vertical wind shear and the rightward motion/redevelopment of convection relative to the mean background wind flow in the column. Furthermore, it is generally accepted that an environment rich in horizontal vorticity oriented in a streamwise manner favors the intensification of supercells into me-
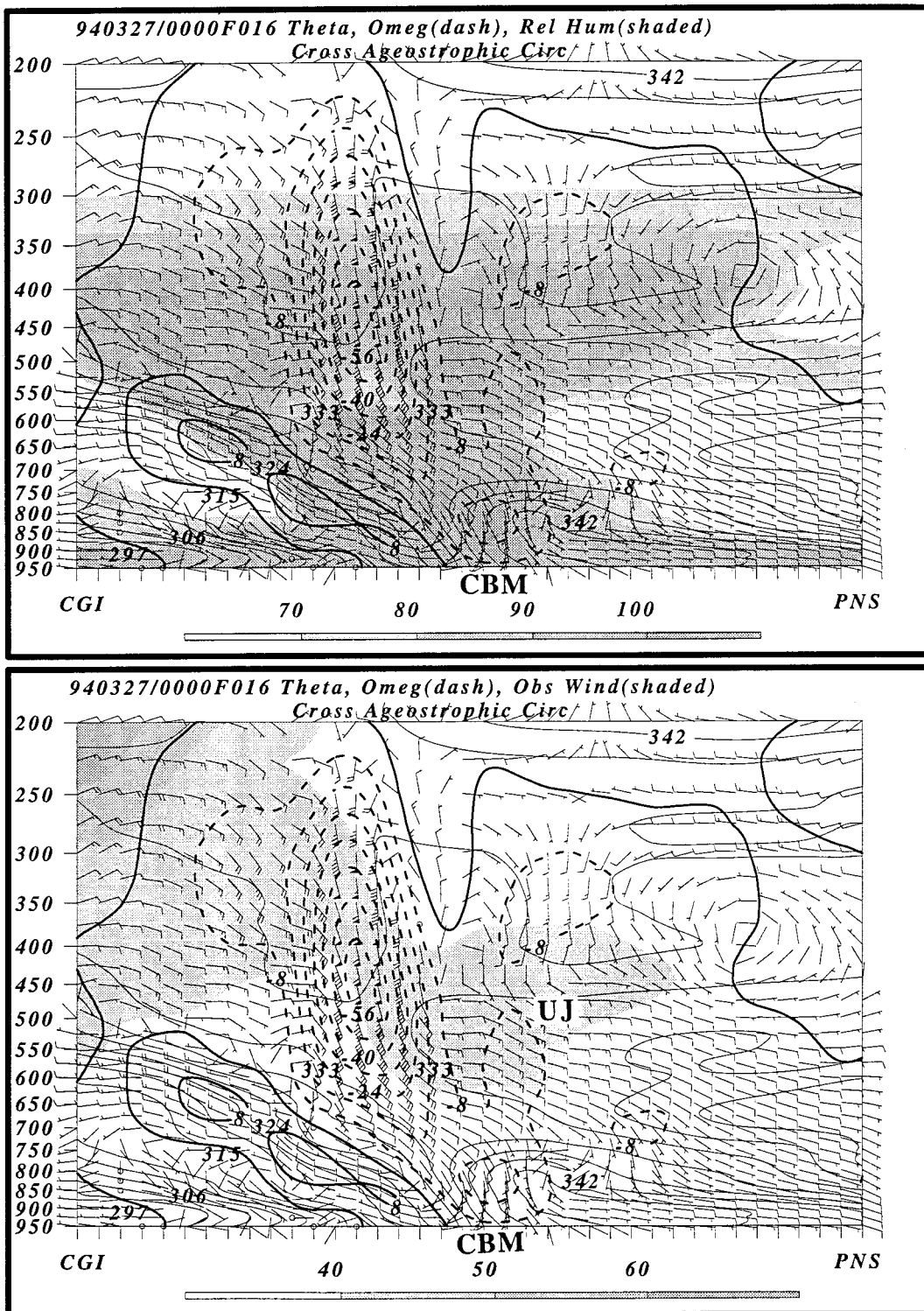
FIG. 27. (a) Same as Fig. 12 but valid at 1600 UTC 27 March 1994. (b) Same as (a) except shading depicts the total wind isotachs in 10 m s^{-1} intervals beginning at 40 m s^{-1}. Here UJ is the unbalanced jetlet.
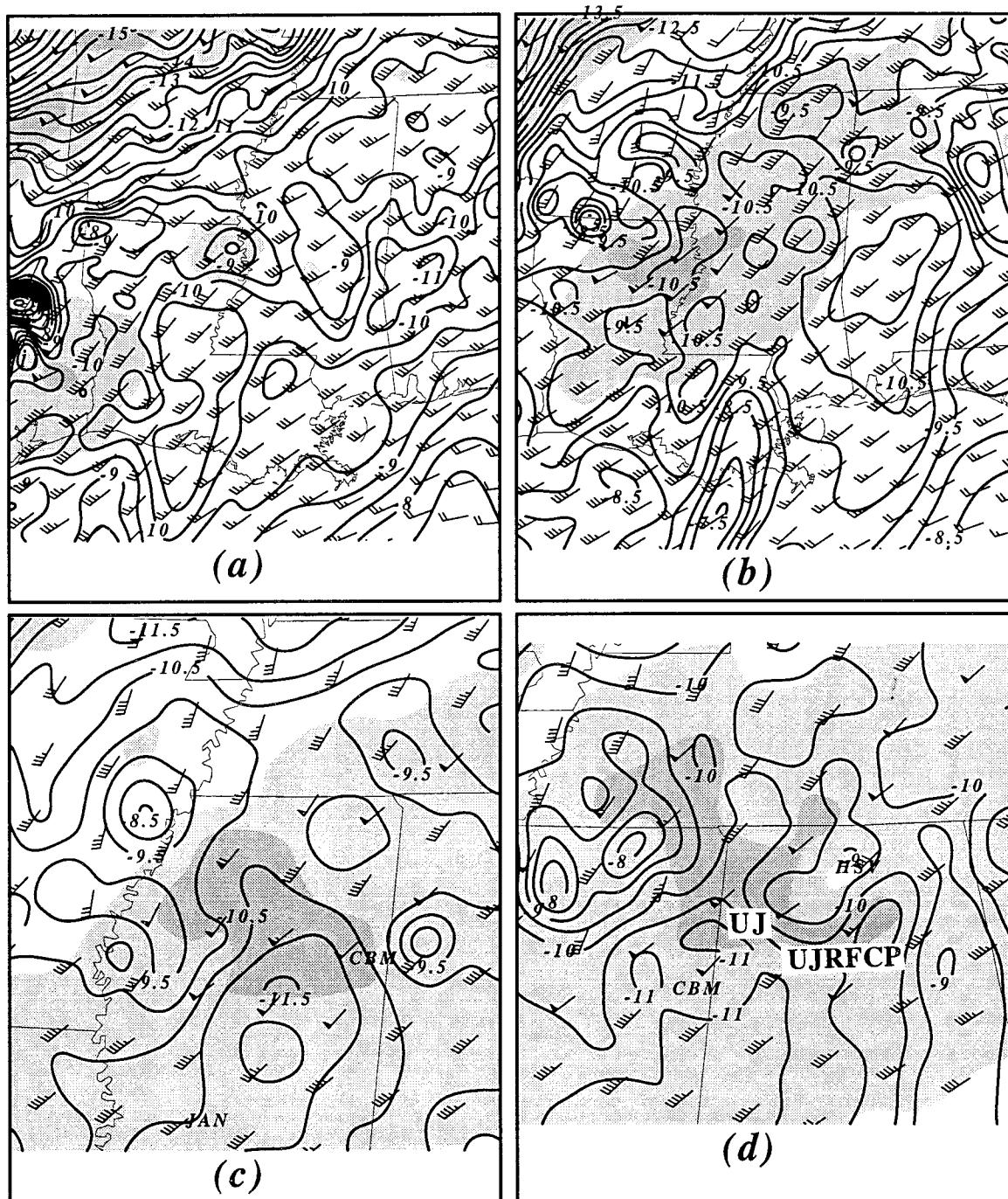
FIG. 28. MASS fine-mesh simulation 500-mb temperature (°C) and 500-mb isotachs (as in Fig. 23) valid at (a) 1200, (b) 1500, (c) 1700, and (d) 1800 UTC 27 March 1994. UJRFCP is the unbalanced jetlet right foreward cold pool.

socyclones that may produce tornadoes (e.g., Wicker 1996). It should be noted, however, that in this hydrostatic meso-beta-scale simulation, explicit details of storm-scale/supercell dynamics are not resolvable. Therefore, it is often questionable to directly apply storm-scale dynamics to the motions of hydrostatic MCS. However, to a first approximation, we are hypothesizing that the use of SRH, which is derived from this hydrostatic simulation, may have utility when employed to forecast regenerating intense MCSs within which individual storms become more supercellular and long lived.

a. Observations

The only observed data available to shed light on the increase of SRH and the low-level horizontal vorticity in proximity to the severe weather involves the surface observations, MGM/XMR profiler, and the 1800 UTC CKL sounding. The surface flow at MGM/XMR does increase during the morning from the south, while the MGM/XMR profiler indicates a gradual increase of southwesterly wind flow at ~3000 m between 1430 and 1530 UTC. Also, the 1800 UTC CKL sounding indicates an increase in 700-mb flow to ~32 m s⁻¹. This should be contrasted with the earlier 1200 UTC observations that indicate weaker values of winds at both levels and somewhat weaker directional shear. Thus, the vertical wind shear is increasing in time. Also, it should be noted that convective cell motion is to the right of the mean column flow at CKL indicating an environment with significant values of SRH.

b. Simulations

Figures 20–21 and 25–29 define how the nested-grid simulation indicates that the vertical wind shear and static stability are rapidly changing during the 1200–1800 UTC time period. These changes produce an environment favorable for juxtaposed SRH increases with low-level horizontal vorticity increases over central Alabama during the 1200–1800 UTC time period. Figures 21 and 25 indicate that during the 1200–1800 UTC period, as the NM moves northeastward from northwestern Louisiana to northern Alabama, the south–southeasterly flow initially over southwestern Louisiana near LCH in its right front quadrant becomes more easterly as the low tracks over central Mississippi near JAN and eventually north-central Alabama between MGM/XMR and HSV. This is quite apparent in Figs. 25c,d as the low-level UJSC becomes better organized in response to the deepening surface low (NM) under the right front flank of the UJ. Simultaneously, the 700-mb flow accompanying the propagating unbalanced jetlet's right exit region, that is, the UJCM depicted in Figs. 21c,d, increases from ~30 to ~40 m s⁻¹ over north-central Alabama between MGM/XMR and HSV with only a slight increase of the southerly component relative to the westerly component. Hence, the vertical shear increases by ~10 m s⁻¹ or by ~40% accompanying the UJ while the increasing meridional variation of the u wind velocity component within the planetary boundary layer accompanying the UJSC has increased in juxtaposition to the existing west–east variation of the southerly wind component, that is, just south of HSV by 1800 UTC. This increases the northwestward-directed surface flow and both the horizontal and vertical vorticity near HSV during the 1700–1800 UTC period (note Figs. 26c,d) resulting in a local maximum, that is, UJSVM. These horizontal and vertical vorticity

increases are in proximity to the region of increasing vertical wind shear within the divergent right front quadrant of the unbalanced jetlet, that is, accompanying the UJCM, and are located primarily along the stream. Furthermore, they are occurring between the RCCF and CF, thus confluence between the two fronts likely produces the local increase in vorticity. The depth of the inflow and increase in vorticity is highlighted by the fact that, as can be seen in Figs. 20c,d, even the 850-mb low-level unbalanced jetlet and its UJCM indicates a developing easterly component underneath the right front quadrant of the midtropospheric jetlet. In effect, the increasing easterly surface wind component offsets the increasing southerly 700-mb wind component while the total wind velocity shear increases substantially resulting in SRH increases over northcentral Alabama by 1800 UTC. The estimated storm vector used in the SRH calculation is 22 m s⁻¹ from 240° (Koch et al. 1998). SRH at HSV increases from 480 to 559 m² s⁻² during the 1700–1800 UTC time period. This SRH maximum (SRHM) closely follows the observed path of the complexes of violent supercells that produced many of the most severe tornadoes (note the vertical vorticity maximum at HSV in Fig. 26d).

These kinematical wind shear changes resulting in increased SRH and vorticity values are supplemented by bouyancy changes accompanying the unbalanced jetlet circulation. As can be seen in Figs. 24 and 28, as the outflow within the right front quadrant of the midtropospheric unbalanced jetlet increases in the jetlet's propagation from east Texas to northwestern Alabama, ascent transports potentially colder air parcels vertically, resulting in concentric 500-mb cooling maxima ahead of 500-mb warming maxima caused by latent heating. The right flank cooling (note UJRFA in Figs. 24g,h and UJRFCP in Figs. 28c,d) combined with the transport of drier air from the southwest (note UJRRDT in Figs. 29c,d) into the propagating jetlet result in the decrease in static stability downstream to the right of the propagating jetlet. This rightward shift in the destabilization of the column enhances the redevelopment of convective systems to the right of the mean advective flow in the column, which is from the southwest, that is, from ~225°. Thus, new convective systems are stimulated to develop to the right of ~225°. The midtropospheric cold pool of most interest, that is, the UJRFCP depicted in Figs. 28c,d, which is located just southeast of HSV at 1800 UTC, can be traced backward in space and time to near CKL at 1700 UTC, southwest of CBM at 1500 UTC, and then back to south-central Louisiana near AEX at 1200 UTC; hence it is located within the right front flank of UJ coincident with the UJRFA feature in the vertical motion field depicted in Figs. 24g,h. Said cold pool is located just downstream from the dry tongue (UJRRDT) depicted in Figs. 29c,d, which is approaching the right flank of the unbalanced jetlet from
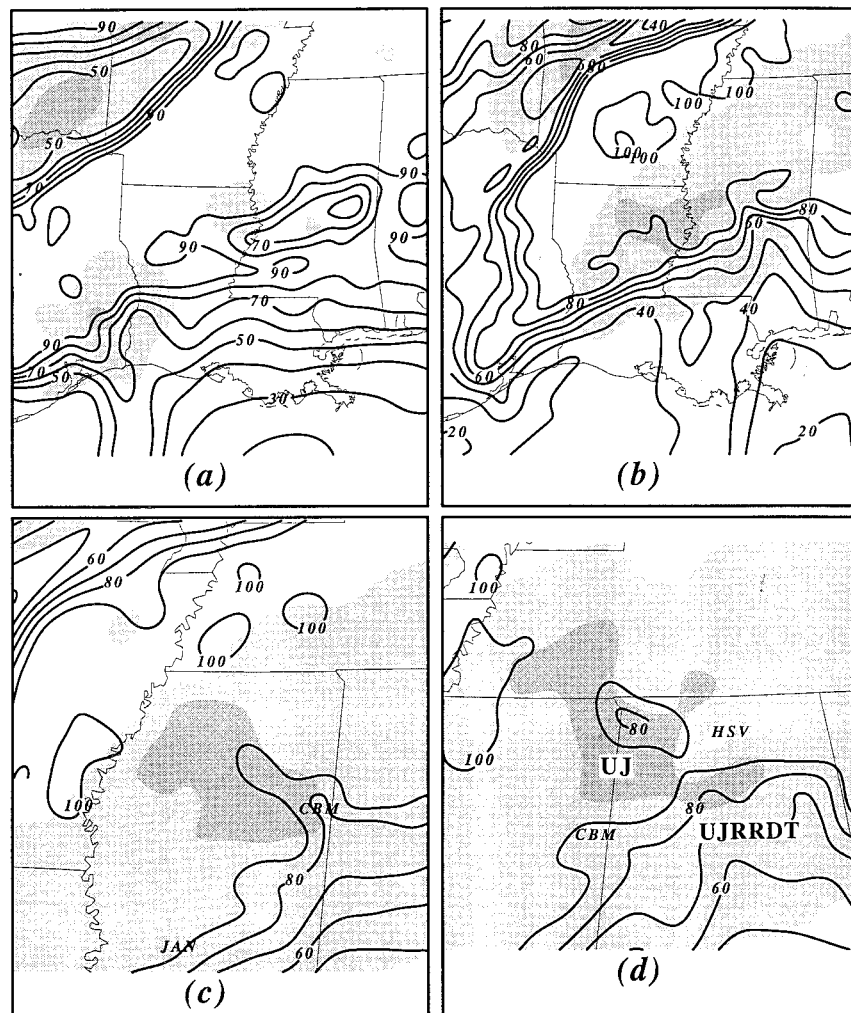
FIG. 29. MASS fine-mesh simulated 700-mb relative humidity (%) and 500-mb isotachs (as in Fig. 23) valid at (a) 1200, (b) 1500, (c) 1700, and (d) 1800 UTC 27 March 1994. UJRRDT is the unbalanced jetlet right rearward dry tongue.

the southwest thus acting to enhance the decrease in static stability as it overides the UJSC and its attendant near-surface inflow depicted in Fig. 25d. Again, most of these key features, that is, the UJCM and NM in Fig. 20, the UJCM in Fig. 21, the UJLDA in Fig. 23, the UJS in Fig. 24, the UJRFA also in Fig. 24, the UJSC and NM in Fig. 25, the UJSVM in Fig. 26, the UJRFCP in Fig. 28, and the UJRRDT in Fig. 29 can be traced backward in space and time to the propagating jetlet and its attendant low-level adjustments that track from northern Louisiana to northern Alabama. This motion is relatively consistent with the surface observations depicted in Fig. 16 and the increase in midlevel wind flow depicted in the JAN and CKL soundings in Fig. 17.

c. Summary

There are several ways in which the unbalanced structure of the simulated midtropospheric jetlet can enhance

SRH as well as the intensity of the low-level horizontal and vertical vorticities. First, the rightward displacement of convection is facilitated as ascent and adiabatic cooling in the right front quadrant reduces the distance high convective available potential energy air in the planetary boundary layer must be transported in order to be destabilized. Second, accelerations in the right front quadrant force vertical wind shear and surface pressure falls due to mass flux divergence farther to the right. Third, the descending air in the right entrance region allows downward momentum fluxes and dry air to be rightward-shifted and closer to the destabilized right front quadrant. Fourth, and finally, since the unbalanced jetlet may evolve into an internal gravity wave, the vertical wind shear effects can be propagated well downstream and to the right of the mean wind. Again, it should be emphasized that we are only applying this SRH-based predictor for use in forecasting hydrostatic convective ensembles, that is, MCS features.

6. Overall summary and conclusions

This paper employs observations and mesoscale numerical simulation model output to define a multistage paradigm for use in predicting severe weather in the southeastern United States with possible application to other parts of the country as well. The base upon which this paradigm is founded involves the juxtapositioning of transverse secondary circulations accompanying the exit region of the STJ and entrance region of the PJ. The low-level return branch circulations accompanying these two juxtaposed jet streaks have the capability to produce intense cross-stream frontal zones when warm continental air accompanying the low-level return branch of the STJ exit region is advected in proximity to cold polar air accompanying the low-level return branch of the entrance region of the PJ. This brings two very dissimilar air masses together, producing very strong cross-stream gradients of temperature within the lower troposphere. If maritime tropical air is overrun by the continental air, latent heating as well as evaporational cooling accompanying precipitation within MCS near the polar and "continental" fronts can produce diabatic perturbations to the cross-stream frontal boundaries. As a result of these processes, regions of extraordinary accelerative flow or mesoscale jetlets develop due to the extraordinary pressure gradient forces produced by the juxtapositioning of different air masses and diabatic perturbations.

The mesoscale jetlets are different from the balanced jet streaks that formed them. Since the mass adjusts to the wind at the sub-Rossby radius of deformation length scales of the mesoscale frontal zones, the exit region of the jetlets are regions of extreme thermal wind imbalance. These accelerating mesoscale jetlets are the products of increasing cross-stream pressure gradients within regions of mesoscale temperature variation. The unbalanced jetlet structure can be seen depicted in Fig. 30. The distribution of vertical motions, acceleration vectors, velocity divergences, and circulations is opposite of that in the UJ79 model depicted in Fig. 1a and is also different from semigeostrophic curved and baroclinically modified jet streaks.

This unbalanced jetlet can be a formidable severe weather-producing feature. Since accelerating and ascending flow can occur within its right front quadrant accompanying a propagating MCS, the right flank adiabatic cooling produces destabilization closer to the maritime tropical air than does the UJ79 paradigm, thus stimulating redevelopment of convective ensembles to the right of the mean wind. Furthermore, the development of streamwise vorticity through intensifying vertical wind shear and low-level inflow is facilitated by the rightward-shifted accelerating flow that, when combined with rightward redeveloping convection, effectively stimulates rapidly increasing storm-relative helicity.

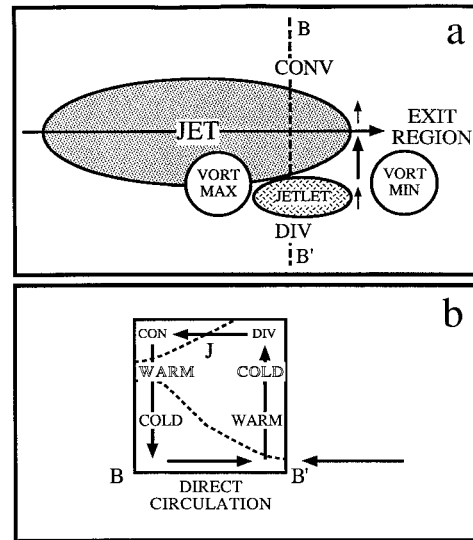This new synoptic/dynamical overview breaks from

Fig. 30. Schematic depicting the (a) horizontal and (b) vertical structures of the unbalanced jetlet. The primary jet shown is the polar jet streak. In (b), the outlined warm/cold temperatures aloft indicate the result of descending/ascending motions transverse to the jetlet.

previous severe storm organization theories by assigning much more active roles to three physical features that establish and are associated with unbalanced flow regimes: 1) the low-level return branch of the STJ, 2) the frontogenetical role of continental air caught up in the STJ low-level return branch rather than its previous assignment as simply a "lid" or simply an elevated mixed layer-producer (e.g., Lanicci and Warner 1991a–c) constrained only to enhancing the convective instability, and 3) the role of geostrophic adjustment processes in inducing rapid accelerative flow within the exit region of a jetlet.

REFERENCES

Bauman, W. H., III, M. L. Kaplan, and S. Businger, 1997: Nowcasting convective activity for space shuttle landings during easterly flow regimes. *Wea. Forecasting,* **12,** 78–107.

Browning, K. A., and R. J. Donaldson Jr., 1963: Airflow and structure of a tornadic storm. *J. Atmos. Sci.,* **20,** 533–545.

Daley, R., 1991: *Atmospheric Data Analysis.* Cambridge University Press, 457 pp.

Davies-Jones, R. P., 1984: Streamwise vorticity: The origin of updraft rotation in supercell storms. *J. Atmos. Sci.,* **41,** 2991–3006.

Fawbush, E. J., R. C. Miller, and L. G. Starrett, 1951: An empirical method of forecasting tornado development. *Bull. Amer. Meteor. Soc.,* **32,** 1–9.

Gonski, R. F., B. P. Woods, and W. D. Korotky, 1989: The Raleigh tornado—28 November 1988: An operational perspective. Preprints, *12th Conf. on Weather Analysis and Forecasting,* Monterey, CA, Amer. Meteor. Soc., 173–178.

Hales, J. E., and M. D. Vescio, 1996: The March 1994 tornado outbreak in the Southeastern United States: The forecast process from an SPC perspective. Preprints, *18th Conf. on Severe Local Storms,* San Francisco, CA, Amer. Meteor. Soc., 32–36.

Hamilton, D. W., Y.-L. Lin, R. P. Weglarz, and M. L. Kaplan, 1998: Jetlet formation from diabatic forcing with applications to the 1994 Palm Sunday tornado outbreak. *Mon. Wea. Rev.,* 2061–2089.

House, D. C., 1963: Forecasting tornadoes and severe thunderstorms. *Severe Local Storms, Meteor. Monogr.,* No. 27, Amer. Meteor. Soc., 141–155.

Kaplan, M. L., and D. A. Paine, 1977: The observed divergence of the horizontal velocity field and pressure gradient force at the mesoscale: Its implications for the parameterization of three-dimensional momentum transport in synoptic-scale numerical models. *Beitr. Phys. Atmos.,* **50,** 321–330.

——, and V. M. Karyampudi, 1992a: Meso-beta scale numerical simulations of terrain drag-induced along-stream circulations. Part I: Midtropospheric frontogenesis. *Meteor. Atmos. Phys.,* **49,** 133–156.

——, and ——, 1992b: Meso-beta scale numerical simulations of terrain drag-induced along-stream circulations. Part II: Concentration of potential vorticity within dryline bulges. *Meteor. Atmos. Phys.,* **49,** 157–185.

——, J. W. Zack, V. C. Wong, and J. J. Tuccillo, 1982: Initial results from a mesoscale atmospheric simulation system and comparisons with the AVE-SESAME I data set. *Mon. Wea. Rev.,* **110,** 1564–1590.

——, R. A. Rozumalski, R. P. Weglarz, Y.-L. Lin, S. Businger, and R. F. Gonski, 1995: Numerical simulation studies of the mesoscale environment conducive to the Raleigh tornado. NOAA Tech. Memo. NWS ER-90, 101 pp. [Available from National Weather Service, Raleigh Forecast Office, 1005 Capability Dr., Raleigh, NC 27695.]

——, Y.-L. Lin, D. W. Hamilton, and R. A. Rozumalski, 1996: The numerical simulation of an unbalanced jetlet and its role in the Palm Sunday 1994 tornado outbreak in Alabama and Georgia. Preprints, *18th Conf. on Severe Local Storms,* San Francisco, CA, Amer. Meteor. Soc., 240–244.

——, S. E. Koch, Y.-L. Lin, R. P. Weglarz, and R. A. Rozumalski, 1997: Numerical simulations of a gravity wave event over CCOPE. Part I: The role of geostrophic adjustment in mesoscale ageostrophic jetlet formation. *Mon. Wea. Rev.,* **125,** 1185–1211.

Keyser, D., and M. A. Shapiro, 1986: A review of the structure and dynamics of upper-level frontal zones. *Mon. Wea. Rev.,* **114,** 452–499.

Koch, S. E., and P. B. Dorian, 1988: A mesoscale gravity wave event observed over CCOPE. Part III: Wave environment and probable source mechanisms. *Mon. Wea. Rev.,* **116,** 2570–2592.

——, D. W. Hamilton, D. Kramer, and A. Langmaid, 1998: Mesoscale dynamics in the Palm Sunday tornado outbreak. *Mon. Wea. Rev.,* **126,** 2031–2060.

Langmaid, A. H., A. J. Riordan, and M. Vescio, 1996: Mesoscale analysis and ETA model perspective of the 1994 Palm Sunday tornado outbreak. Preprints, *18th Conf. on Severe Local Storms,* San Francisco, CA, Amer. Meteor. Soc., 37–41.

Lanicci, J. M., and T. T. Warner, 1991a: A synoptic climatology of the elevated mixed layer inversion over the southern Great Plains in spring. Part I: Structure, dynamics, and seasonal evolution. *Wea. Forecasting,* **6,** 181–197.

——, and ——, 1991b: A synoptic climatology of the elevated mixed layer inversion over the southern Great Plains in spring. Part II: The life cycle of the lid. *Wea. Forecasting,* **6,** 198–213.

——, and ——, 1991c: A synoptic climatology of the elevated mixed layer inversion over the southern Great Plains in spring. Part III: Relationship to severe storms climatology. *Wea. Forecasting,* **6,** 214–226.

Mahrt, L., and H. Pan, 1984: A two-layer model of soil hydrology. *Bound.-Layer Meteor.,* **29,** 1–20.

Manobianco, J., J. W. Zack, and G. E. Taylor, 1996: Workstation-based real-time mesoscale modeling designed for weather support to operations at the Kennedy Space Center and Cape Canaveral Air station. *Bull. Amer. Meteor. Soc.,* **77,** 653–672.

MESO, 1993: MASS version 5.8 reference manual, 118 pp. [Available from MESO Inc., 185 Jordan Road, Troy, NY 12180.]

Newton, C. W., 1963: Dynamics of severe convective storms. *Severe Local Storms, Meteor. Monogr.,* No. 27, Amer. Meteor. Soc., 33–58.

Noilhan, J., and S. Planton, 1989: A simple parameterization of land surface processes for meteorological models. *Mon. Wea. Rev.,* **117,** 536–549.

Shapiro, M. A., 1981: Frontogenesis and geostrophically forced secondary circulations in the vicinity of jet stream-frontal zone systems. *J. Atmos. Sci.,* **38,** 954–973.

Uccellini, L. W., and D. R. Johnson, 1979: The coupling of upper- and lower-tropospheric jet streaks and implications for the development of severe convective storms. *Mon. Wea. Rev.,* **107,** 662–673.

——, and S. E. Koch, 1987: The synoptic setting and possible energy sources for mesoscale wave disturbances. *Mon. Wea. Rev.,* **115,** 721–729.

——, and P. J. Kocin, 1987: The interaction of jet streak circulations during heavy snow events along the east coast of the United States. *Wea. Forecasting,* **2,** 289–308.

——, R. A. Petersen, K. F. Brill, P. J. Kocin, and J. J. Tuccillo, 1987: Synergistic interactions between an upper-level jet streak and diabatic processes that influence the development of a low-level jet and a secondary coastal cyclone. *Mon. Wea. Rev.,* **115,** 2227–2261.

Whitney, L. F., 1977: Relationship of the subtropical jet stream to severe local storms. *Mon. Wea. Rev.,* **105,** 398–412.

Wicker, L. J., 1996: The role of near surface wind shear on low-level mesocyclone generation and tornadoes. Preprints, *18th Conf. on Severe Local Storms,* San Francisco, CA, Amer. Meteor. Soc., 115–119.

Zack, J. W., and M. L. Kaplan, 1987: Numerical simulations of the subsynoptic features associated with the AVE-SESAME I case. Part I: The preconvective environment. *Mon. Wea. Rev.,* **115,** 2367–2394.

——, C. A. Mattocks, and M. D. Bousquet, 1991: A statistical-dynamical mesoscale thunderstorm forecast system for the Kennedy Space Center. Preprints, *Ninth Conf. on Numerical Weather Prediction,* Denver, CO, Amer. Meteor. Soc., 447–450.

Zang, D.-L., and R. A. Anthes, 1982: A high resolution model of the planetary boundary layer-sensitivity tests and comparisons with SESAME-79 data. *J. Appl. Meteor.,* **21,** 1594–1609.